



## Retrieval of suspended sediment concentration (SSC) in the Arabian Gulf water of arid region by Sentinel-2 data

Rajendran Sankaran<sup>a,\*</sup>, Jassim A. Al-Khayat<sup>a</sup>, Aravinth J<sup>b</sup>, Mark Edward Chatting<sup>c</sup>, Fadhil N. Sadooni<sup>a</sup>, Hamad Al-Saad Al-Kuwari<sup>a</sup>

<sup>a</sup> Environmental Science Center, Qatar University, P.O. Box: 2713, Doha, Qatar

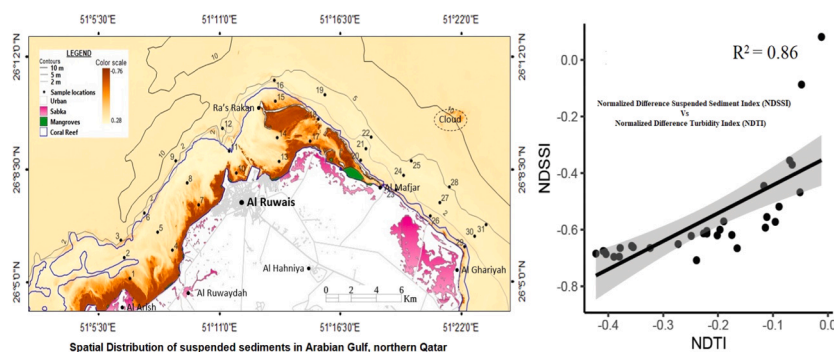
<sup>b</sup> Department of Electronics and Communication Engineering, Amrita School of Engineering, Coimbatore, Amrita Vishwa Vidyapeetham, India

<sup>c</sup> School of Civil Engineering University College Dublin, Ireland

### HIGHLIGHTS

- Mapping of suspended sediments is carried out using Sentinel-2 data and indices.
- Regression analyses showed a strong relationship of  $R^2 = 0.95$  among used indices.
- Satellite-derived results are validated by field studies and in-situ measurements.
- Grain size, minerals, and major and trace elements of sediments are studied.
- Uses of sensors and indices are demonstrated to map SSC in Gulf water, arid region.

### GRAPHICAL ABSTRACT



### ARTICLE INFO

Editor: Ouyang Wei

#### Keywords:

Suspended sediment concentration  
Gulf water  
Sentinel-2  
Spectral indices  
Qatar  
Arabian Gulf

### ABSTRACT

Suspended sediment concentration (SSC) in water increases temperature and turbidity, limits the photosynthesis of aquatic plants, and reduces biologically available oxygen. It is important to study SSC in the coastal waters of the Arabian Gulf. Thus, this study mapped the SSC of coastal water between Al Arish and Al Ghariyah in northern Qatar using the spectral bands of the MultiSpectral Imager (MSI) of Sentinel-2 by calculating the Normalized Difference Suspended Sediment Index and Normalized Suspended Material Index. The results are studied using the Normalized Difference Turbidity Index and Modified Normalized Difference Water Index. The mapping of SSC in the water using NDSSI showed the presence of a high concentration of suspended sediments between Al Arish and Al Mafjar and a low concentration between Al Mafjar and Al Ghariyah. The mapping of NSMI showed values between 0.012 (clear water) and 0.430 (more suspended material) for the occurrence of suspended materials and supported the results of NDSSI. The study of turbidity using an NDTI image showed turbidity index values ranging from  $-0.44$  (clear water) to  $0.12$  (high turbidity) and confirmed the occurrence and distribution of suspended sediments and materials in the water. The MNDWI image was able to discriminate clear water with bright pixels from silty sand and mud flats. The relationships between NDSSI, NSMI, and NDTI were correlated with in-situ measurements and studied to find suitable indices to map SSC. Regression analyses showed the strongest relationship between NSMI and NDTI ( $R^2 = 0.95$ ) next to NDSSI and NDTI, where NDTI had the

\* Corresponding author.

E-mail address: [srajendran@qu.edu.qa](mailto:srajendran@qu.edu.qa) (R. Sankaran).

<https://doi.org/10.1016/j.scitotenv.2023.166875>

Received 20 March 2023; Received in revised form 4 September 2023; Accepted 4 September 2023

Available online 6 September 2023

0048-9697/© 2023 The Authors. Published by Elsevier B.V. This is an open access article under the CC BY license (<http://creativecommons.org/licenses/by/4.0/>).

strongest effect on NDSI ( $R^2 = 0.86$ ). The satellite data results were evaluated by studying the physical parameters and spatial distribution of suspended sediments in the surface and bottom waters. In addition, the grain size distributions, mineral identification, and chemical element concentrations in the bottom sediment samples were studied.

## 1. Introduction

Optical sensors of different satellite platforms are capable of recording radiation from the water's surface of the earth to provide information about the physicochemical properties of water such as turbidity (the cloudiness in water caused by suspended solids, measured in NTU; Frayne, 2010), suspended sediment concentration (SSC) (the clay, silt, and sand and organic matter in water quantified in mg/l; Vanacker, 2011), total suspended solids (TSS) (the total solids in water that can be trapped by a filter, quantified in mg/l; Torres-Vera, 2023), total organic carbon (TOC) (the amount of bound carbon in waterborne organic compounds, quantified in mg/l C; Sillanpää et al., 2018), (Saberioon et al., 2020; Silveira Kupssinskü et al., 2020; Zhang et al., 2022; Kabir and Ahmari, 2020; Peterson et al., 2018), and microbiological properties like Chlorophyll-a (Chl-a) contents (Saberioon et al., 2020; Dörnhöfer et al., 2018). Researchers also used data from satellites and UAVs having different resolutions to map and quantify such properties of waters that occurred in land and coastal regions. These include airborne platforms such as AVIRIS and CASI (Jensen et al., 2019; Hunter et al., 2010), unmanned aerial vehicles (Guimares et al., 2019), and satellites like Sea-WiFS (Gohin et al., 2019), MERIS (Steinmetz et al., 2011), MODIS (McCullough et al., 2012), Landsat (Smith et al., 2021; Hossain et al., 2021; Shahzad et al., 2018), SPOT (Gernez et al., 2015), Quickbird (Lyons et al., 2011), GeoEye-1 (Randazzo et al., 2020), WorldView-3 (Wilson et al., 2022) and Sentinel-2 (Rajendran et al., 2022; Wilson et al., 2022).

The estimation of SSC has been carried out successfully using reflectance data of optical sensors in the lacustrine and estuarine environments based on in-situ measurements. Binding et al. (2005) estimated SSC from color measurements in moderately turbid ocean waters. They analyzed the impact of variable particles that have scattering properties. Wang and Lu (2010) estimated the suspended sediment concentration of the Lower Yangtze River, China using Terra MODIS. They demonstrated the accurate estimation of SSC using bands 2 and 5 where atmospheric conditions were unknown. Liu et al. (2017) used MSI bands to retrieve suspended particulate matter concentrations in Poyang Lake, China. Peterson et al. (2018) studied suspended sediment concentration and estimated it from Landsat Imagery along the Lower Missouri and Middle Mississippi Rivers using an Extreme Learning Machine algorithm. Pahlevan et al. (2019) evaluated and compared the suitability of Landsat 8 and Sentinel-2A/B data to study the TSS. They stated that the OLI and MSI offer more spectral measurements within the near-infrared (NIR) region to estimate TSS. Kabir and Ahmari, (2020) studied the water radiance and suspended sediment concentration using digital imagery and described an algorithm for a more accurate estimation of SSC in riverine environments. Silveira Kupssinskü et al. (2020) used supervised Machine Learning algorithms to predict the concentration of suspended solids and chlorophyll-a and evaluated them with R-squared values above 0.8. Satellite data are also well utilized and mapping of SSC is carried out using several satellite data indices (Yunus et al., 2022; Kavan et al., 2022; Chalov et al., 2021; Hafeez et al., 2021; Garg et al., 2020; Balasubramanian et al., 2020). Park and Latrubesse (2014) modeled suspended sediment distribution patterns of the Amazon River using MODIS data. They stated that the study successfully demonstrated the capability of MODIS based model to capture the spatial and temporal variability of surface sediments. Their empirical models derived between field surface sediment concentration and surface reflectance data showed  $0.79 < R^2 < 0.92$ . Chalov et al. (2021) stated that the MODIS Terra and Aqua are considered suitable for

identifying trend dynamics of surface sediment distribution on a large spatial scale due to their daily coverage and long archive. Recently, Yunus et al. (2022) studied the climate change and anthropogenic activities on the suspended sediment dynamics in Asian estuaries. They analyzed trends of SSC (2000–2020) at the mouths of 10 major Asian rivers using 10 available satellite-SSC algorithms. They stated that their results showed the presence of anthropogenic activities that threaten the marine ecosystem more than climate forcing on the Asian coasts.

Kavan et al. (2022) used Sentinel-2 data and studied sediment fluxes in the Largest Glacial Lake in Svalbard to Fjord System. They stated that the suspended sediment indices can be used for the quantification of sediment flux in the fjord of coastal environments. Zhang et al. (2022) estimated the SSC of Yangtze Main stream based on Sentinel-2 MSI Data. They developed a method to retrieve SSC that is suitable for rivers and estimated SSC with in situ measurements. Their results showed a root mean squared error (RMSE) of 24.87 mg/l and a mean relative error (MRE) of 51.91 %. Pahlevan et al. (2022) studied the optical water quality of chlorophyll-a (Chl-a) and TSS and showed absorption of dissolved organic matter at 440 nm using Landsat-8 (OLI), Sentinel-2 (MSI), and Sentinel-3 (OLCI) data. They estimated the TSS from these three missions and stated that the mapping of Chl-a using OLCI and MSI achieved greater accuracy than those from OLI. However, no significant studies on mapping of SSC have been performed along coastal regions of the Arabian Gulf. Therefore, the present study aims to map the suspended sediment concentration in the coastal water of northern Qatar, situated in the Arabian Gulf under an arid environment, using Multi-Spectral Imager (MSI) data of Sentinel-2 and derived indices to assess the occurrence of suspended sediments and to understand the turbidity, coastal erosion and coastline changes along the coastline. The study evaluates the imagery results of SSC with the results of field studies, in-situ measurements, and laboratory analyses.

## 2. Study area

The Arabian Gulf (also known as the Persian Gulf) is situated between latitudes  $24^\circ$  and  $30^\circ$ N and longitudes  $48^\circ$  and  $57^\circ$ E. The Gulf is a semi-enclosed sea, extending 1000 km from the Shatt Al-Arab waterway (Iraq) to the Strait of Hormuz with varying widths from 75 to 350 km. It has an area of about 239,000 km<sup>2</sup> with an average depth of about 36 m (100 m maximum depth). The gulf is surrounded mainly by Arab countries, namely the United Arab Emirates, Qatar, Saudi Arabia, Kuwait, Iraq, and Iran. The area of present study is the coast of Al Arish - Al Ghariyah situated in the northern part of Qatar ( $26^\circ 5'$  and  $26^\circ 12'$ N latitude;  $51^\circ 22'E$  and  $51^\circ 5'E$  longitude) (Fig. 1). Qatar has a desert climate with two transition periods as very mild winters (December to March) and hot summers (June to September) (Al Senafi and Anis, 2015). Here, the temperatures attain  $51^\circ$  C in summer and low as  $15^\circ$  C during winter (Govinda Rao et al., 2001). The coastal waters of the region are hottest in August when the surface temperature of the sea exceeds  $30^\circ$  C. The winds over the Gulf vary between northwest (NW) to north (N) throughout the seasons while east (E) to southeast (SE) winds prevail occasionally (Thoppil and Hogan, 2010). The strongest winds in the Gulf are associated with Shamal events (Yu et al., 2016). They are two kinds 1) shorter events of 24–36 h and 2) longer events of 3–5 days based on their intensity and spatial distribution (Aboobacker et al., 2011). The currents and storm surges in coastal areas are influenced mainly by northwesterly “shamal” winds (Cavalcante et al., 2016). El-Sabh and Murty (1989) studied the storm surge phenomenon in the Arabian Gulf through the development of mathematical models. Their

results showed that the Gulf is subject to major negative and positive storm surges. They stated that the strong winds associated with the Shamal system, atmospheric pressure gradients, topography, and tidal effects can raise water level deviations by several meters. Li et al. (2020) studied the mean wave periods (Tm) in the Gulf and reported between 1.5 and 5.0 s.

In Qatar, the north and east coasts are exposed to the complex interactions of waves, tides, and currents in the Arabian Gulf (Pous et al., 2015). Liao and Kaihatu (2016a, 2016b) stated that wave refraction causes 20 % total energy deviation (TED) along the north-eastern corner of Qatar during winter. Al-Yousef (2003) stated that the tides along the eastern coast of Qatar are mixed diurnal, with ranges of 1.1–2.3 m. The surface currents along this coast are tidally driven and move generally southward and offshore at <10 cm/s (Pous et al., 2013; Lardner et al., 1988). Aboobacker et al. (2021) analyzed wave parameters off Fuwairit, the north coast of Qatar, and identified the features associated with different wind systems. Their results showed that Nashi winds influence the east and northeast coasts of Qatar with higher waves than those generated by Shamal winds. They described the waves, currents induced tide-driven flows, and regional scale circulations that have significant implications in physical and biogeochemical processes including sediment transport along the coast of Qatar.

The study area has low topography and gentle slopes of bathymetry (Fig. 1) (Purkis and Riegl, 2012). It has high rates of evaporation and a salinity average of 42 ppt (John et al., 1990). Such evaporation and salinity developed sabkhas along the coast and inland in the area (Rajendran et al., 2021a). The other features of the area are saltmarshes, mudflats, and mangroves (Fig. 1) (Rajendran et al., 2022, 2021a, 2021b; Vaughan and Burt, 2016). The mud, clay, and sand sediment deposits have occurred along the coast. These deposits support the growing plants, mangroves, seagrasses, and microbials (Rajendran et al., 2022; Lokier and Fiorini, 2016). The land is a carbonate platform dominated by dolomites and limestones of the Dammam and Rus Formations and the shelf edges are well exposed along the coastline (Al-Saad, 2005).

### 3. Spectral bands characters of SSC

The relationship between spectral band absorptions and SSC is affected by several factors such as depth of water body, bottom reflection, vertical variation in sediment deposits, types, size distribution and composition of sediments, and studied by several researchers (Smith et al., 2021; Kabir and Ahmari, 2020; Rumora et al., 2020). Here, the interface between air and water and the conditions of the atmosphere adds more complexity (Schmugge et al., 2002; Gray et al., 2000). However, Peterson et al. (2018) stated that the reflection coefficient of solar radiation in VNIR and NIR wavelength regions and the amount of sediment in the water is directly related. According to Long and Pavelsky (2013), the higher SSC exhibits a higher reflectance coefficient in a specific spectrum. The bands in visible and NIR regions provide more opportunities to study the optically complex coastal/inland waters (Moses et al., 2009) or extremely turbid waters (Lee et al., 2016; Nechad et al., 2010). The bands can also be used best to retrieve SSC, TOC, Chl-a, and CDOM (Kutser et al., 2016; Toming et al., 2016). Chen et al. (1991) stated that the suspended sediment concentration and reflectance were log-linear at 450 to 700 nm and linear at 700 to 1050 nm wavelengths. Harrington et al. (1992) studied the reflectance of SSC using the NIR band of Landsat MSS 3 and observed a linear relationship in the range of 0 to 500 mg/l and nonlinear at higher SSC. Lodhi et al. (1997) described that the 580 to 690 nm (visible range) provided important information for the type of suspended sediments, and 714 to 880 nm (NIR range) showed best to estimate the amount of sediment in surface waters. Wang and Lu (2010) showed water reflectance in Band 2 (841 to 876 nm) of MODIS data and described the presence of a linear and non-linear relationship for the concentration of suspended sediments in the ranges of 74–600 mg/l and 600–881 mg/l respectively. In addition, water turbidities were estimated by Kuhn et al. (2019) and Dogliotti et al. (2015) using a semi-empirical red band algorithm using 655 nm bands of Landsat 8 and Sentinel-2. Thus, to map and calculate SSC, the spectral bands of sensors in the visible and NIR regions are required with a high signal-to-noise ratio (Caballero et al., 2018). The MSI of Sentinel-

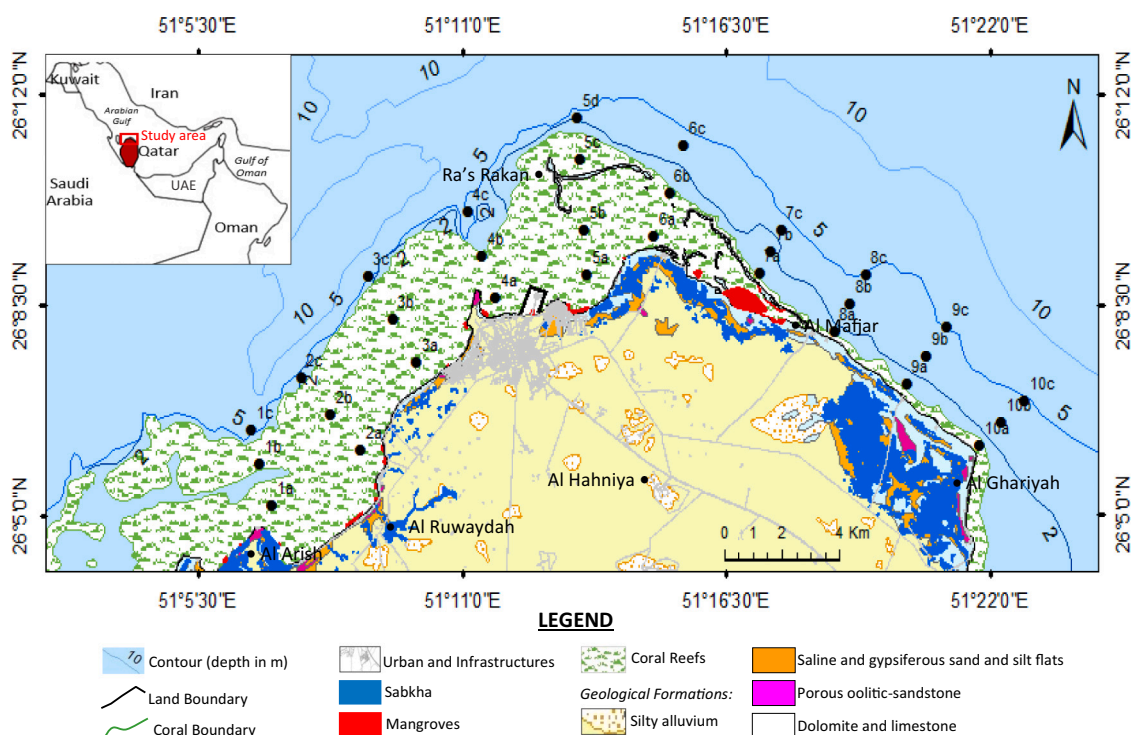


Fig. 1. Study area showing the lithology, coastal features, and sample locations.

2 has these bands at 10 m high spatial resolution and provides a unique perspective on coastal water remote sensing.

Therefore, in this study, we collected image spectra of sample locations of the Al Arish – Al Ghariyah region (Fig. 1) and developed a spectral library using MSI spectral bands, and studied the absorptions and reflectances of the water and suspended sediments of the study area. The spectra of selected locations are given in Fig. 2. The spectral library plot shows that the spectra collected at very shallow depths (< 0.5 m) exhibit spectral absorptions around the blue band (band 2 @ 490 nm; black dashed elliptical) and high reflections around NIR bands from band 7 (Red-edge, 786 nm) to band 8A (NIR-narrow, 865 nm) with absorptions at band 8 (NIR-wide, 842 nm; red dotted). The Center Wavelengths of MSI spectral bands are given in Table 1 in the Supplementary material. The absorptions in the blue region are due to the presence of water, and the reflection and absorption around the NIR region are due to the presence of suspended sediments in the water. The spectra collected at shallow depths (around 1 m) of water show relatively low reflections (see reflectance values) and low absorptions in the blue and NIR regions when compared with the spectra collected at very shallow depths of water (Fig. 2). The overall low reflection among the spectra is due to the depth of water, and the low absorptions in NIR bands may be due to the presence of sediments that occurred at the shallow depth of water. The significant absorptions observed in band 4 (Red, 665 nm) and band 6 (Red-edge2, 740 nm) in the spectra of shallow water are due to the occurrence of Chl-a (Rajendran et al., 2022). It can be interpreted that the spectra collected in the area of shallow water exhibited high reflection around the blue region when compared to the NIR region, which may be due to water reflection at shallow depth and absorption of suspended sediments in the water, respectively. As well as, the spectra collected in deep water (>2 m) show similar absorptions, reflections, and trends of shallow water, and the overall very low reflection in all may be due to the depth of water. The absorptions near the blue and NIR regions are due to the absorptions of water and suspended sediments at the depth (Fig. 2). The green (560 nm) and red-edge (786 nm) bands that occurred near the blue and NIR regions can also be considered to discriminate the water and suspended sediments (Wang and Lu, 2010; Lodhi et al., 1997; Chen et al., 1991). The interpretations and study of spectral band absorptions of MSI bands suggest that the suspended sediments can be mapped using MSI spectral bands of blue, green, and NIR regions.

## 4. Data and methods

### 4.1. Satellite data and pre-processing

The Sentinel-2A and 2B satellites were launched on 23 June 2015 and 7 March 2017 respectively. These are sun-synchronous and polar-orbiting satellites that orbit at 786 km altitude. The MultiSpectral Imager (MSI) of the satellites has 13 bands in the wavelength between 430 nm and 2320 nm and collects information at the spatial resolutions of 10, 20, and 60 m. The radiometric resolution of data is 12-bit. The instrument has a swath width of 290 km and a temporal resolution of a minimum of five days (Drusch et al., 2012). The data of MSI are well utilized by scientists in coastal studies (Zhang et al., 2022; Pahlevan et al., 2022, 2019; Silveira Kupssinskü et al., 2020; Tuuli et al., 2020; Elhag et al., 2019; ESA, 2015). In this study, the cloud-free Sentinel-2B data of December 15, 2020 (S2B\_MSIL1C\_20201215T071309\_N020\_9\_R106\_T39RWJ\_20201215T080630) which was closer to the day of fieldwork, were downloaded from Sentinel's Scientific Data Hub to map the SSC of the study area. The data were preprocessed for radiometric calibration and atmospheric correction using the Sentinel Application Platform (SNAP) program, which has the Sen2Cor plugin and Sentinel-2 Toolbox (<http://step.esa.int/main/toolboxes/snap/>) (Louis et al., 2016; Clevers and Gitelson, 2013; Rajendran et al., 2022). During pre-processing, the data were projected to the UTM Zone 39 N projection reference to the WGS 1984 ellipsoid. The identification of cloud-free pixels was carried out using IdePix (v2.2). All the image analyses are carried out using ENVI image processing software (ENVI 5.5, Harris Geospatial Solutions, CO, USA; <https://www.harrisgeospatial.com>).

### 4.2. Mapping of SSC

Studies are well demonstrated about the suspended sediments in rivers (Zhang et al., 2022; Mohsen et al., 2022; Chalov et al., 2021; Do et al., 2017; Park and Latrubesse, 2014), estuaries (Yunus et al., 2022; Sharples et al., 2017), coasts (Balasubramanian et al., 2020), bays (Yunus et al., 2021), and deltas (Chalov et al., 2019, 2017). The sediments in the coastal water act as conduits for marine life to flourish (Balasubramanian et al., 2020). However, the marine systems and biogeochemical cycle are affected in recent years by river discharge and sediment flux due to the change in climate and the increase in human activities (Yunus et al., 2021; Chalov et al., 2021; Do et al., 2017;

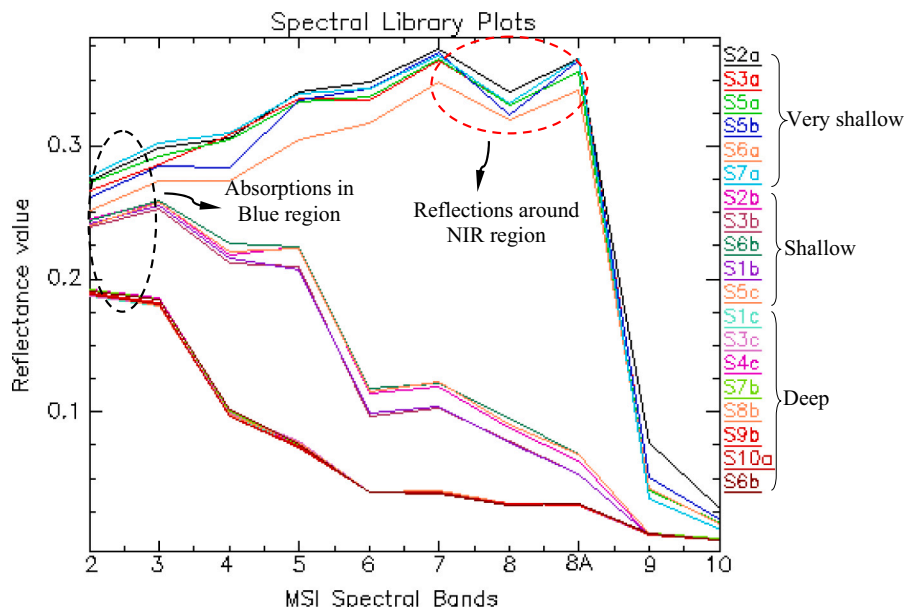


Fig. 2. Spectral plot of MSI bands showing the spectral band absorptions and reflections of water and suspended sediments.

Sharples et al., 2017). The measurement of suspended sediment concentration (SSC) can be done by using conventional laboratory analysis (e.g., gravimetric method) (Moore et al., 2012), optical (e.g., laser in situ scattering and transmissometry) (Guerrero et al., 2017) and acoustic methods (Park and Lee, 2016; Rai and Kumar, 2015). But these methods have several disadvantages including the requirement for more water samples at each location and each depth in the observation station. Though the methods determine SSC accurately, it has limitations and is unable to provide time series data and spatial information about SSC (Tessier et al., 2008; Moore et al., 2012). Moreover, the methods are relatively expensive and time-consuming for the measurement process and sampling at the observation site.

Literature reviews also show the use of single band, band ratios, and spectral indices developed using NIR, red, green, and blue bands to map and estimate suspended sediment concentration (Yunus et al., 2022; Balasubramanian et al., 2020; Feyisa et al., 2014; Doxaran et al., 2009; Lacaux et al., 2007). In this study, mapping of SSC of the study region is carried out using MSI data and index namely Normalized Difference Suspended Sediment Index (NDSSI) (Hossain et al., 2010). The result of mapping is studied further with the occurrence of suspended materials and turbidity of the region using Normalized Suspended Material Index (NSMI) (Montalvo, 2010), Normalized Difference Turbidity Index (NDTI) (Lacaux et al., 2007) and Modified Normalized Difference Water Index (MNDWI) (Xu, 2006) to understand more about SSC of the region. The indices are expressed as below.

$$\text{NDSSI} = (B8 - B2) / (B8 + B2)$$

$$\text{NSMI} = (B4 + B3 - B2) / (B4 + B3 + B2)$$

$$\text{NDTI} = (B4 - B3) / (B4 + B3)$$

$$\text{MNDWI} = (B3 - B11) / (B3 + B11)$$

The NDSSI was introduced by Hossain et al. (2010) using ETM<sup>+</sup> data from Landsat 7. The index calculates the surface reflectance of data to determine the relative clarity of areas within a water body. It uses the blue band which provides the highest reflectance, and the near-infrared band which produces the lowest reflectance values for water. The index is developed by subtracting the near-infrared band (NIR) from the blue band and dividing it by the sum of both bands. To calculate suspended sediments, the index using spectral bands 2 (Blue: 0.458–0.523 μm) and 8 (NIR: 0.785–0.899 μm) for Sentinel-2 data (Kavan et al., 2022). The NDSSI results for SSC values are in the range between –1 to +1, where –1 represents the presence of the highest SSC and 1 represents the lowest SSC (Hossain et al., 2010).

Further, the NSMI was used here to confirm the occurrence of SSC in the coastal region. The index was proposed by Montalvo (2010) and adopted to track the diurnal variability of SSC. It is developed based on the peak of reflectance of water in the blue band and with the concentration of sediments, which increase the reflectance in green and red bands where clean water absorbs radiation rather than reflect (Hafeez et al., 2021; Arisanty and Nur Saputra, 2017). The equation is derived by summing the red and green bands and subtracting the blue band and then dividing the result by the sum of all the bands. It gives values between –1 and +1 where the low values represent clear water and the high values show the presence of more suspended sediments.

We also studied the NDTI (Lacaux et al., 2007) and MNDWI (Xu, 2006) to support the mapping of SSC using NDSSI and NSMI, and to understand the suspended sediment concentration and turbidity in the study region. The NDTI uses the reflectance of red and green bands by understanding that the red band increases reflectance with the increase of turbidity. The reflectance is weak in green (Virtanen et al., 2020). The index is well utilized to generate qualitative turbidity levels based on statistics (Bid and Siddique, 2019; Townshend and Justice, 1986; Tucker and Sellers, 1986). The results of NDTI vary from –0.2 to +0.25, where the low values indicate clear water and the high values represent the

presence of high turbid water (Bid and Siddique, 2019). The NDTI index plays a significant role in identifying turbid water and helps to assess the SSC in the water. The amounts of SSC are usually linearly related to turbidity. This index can be considered an ideal indicator for studying SSC in coastal areas and estuaries (Garg et al., 2020; Elhag et al., 2019).

Moreover, the MNDWI derived image allows us a more precise extraction of water features from vegetation, soil, and land. The index uses green and mid-infrared (MIR) spectral bands. Xu (2006) stated that the MIR band has a greater signature than the green band in the study of spectral reflectance of lake water. He showed the best results using the MIR band instead of using the NIR band using the developed Normalized Difference Water Index (NDWI) by McFeeters (1996). He tested MNDWI with the water types of ocean, lake, and river, and stated that the enhancement MIR in the MNDWI image produced accurate extraction of water features from vegetation, soil, and land features that have negative values. In this study, the MNDWI is used to show the extent of seawater from the coast and other coastal features including mud flats, mangroves, land, and man-made infrastructures (see Fig. 1 in Supplementary material).

#### 4.3. Field sampling and in-situ measurements

The results of the mapping of SSC were verified on the coast of Al Arish - Al Ghariyah by conducting several field studies between 29th November and 15th December 2020, the day closer to Sentinel-2B pass over the area. During the studies, surface and underwater photography were taken, and samples of water were collected using a Niskin sampler over the surface of <0.5 m and bottom to a maximum depth of 7 m at 31 sites using a GPS along the 10 transects across the coast (Fig. 1) (Fig. 2 in Supplementary material; Rajendran et al., 2022). The sites were selected about 1 km distance from the coast towards the offshore to a maximum of 3 km at 5 km intervals on the coastline (Fig. 1). Samples were also collected at a middle depth where the depth of water is above 2 m. The samples of bottom sediments were collected using polythene bags. During sampling, in-situ measurements were also carried out for Ec, pH, temperature, and total dissolved solids at the sites using YSI-EXO2 Multi-Parameter sonde. The total suspended sediments (mg/l) of water samples were calculated using the ASTM D5907 method (<https://www.astm.org/standards/d5907>). The sediment samples were analyzed for major and trace element concentrations by using Inductively Coupled Plasma - Optical Emission Spectrometry (ICP-OES) method. The spatial distribution of suspended sediments, clay and silt, and concentrations of phosphate and sulfate are studied by preparation of contour maps using ArcGIS software (<https://www.arcgis.com>).

#### 4.4. Evaluation and validation

The results of indices were evaluated with the in-situ data to understand the relationship among the indices. A correlation analysis was carried out between the results of NDSSI and NSMI with the results of NDTI and MNDWI indices and field data. The R<sup>2</sup> and RMSE were determined and studied for fitting and accuracies to evaluate the indices and find the suitability of indices in the mapping of SSC. The results are integrated with the spatial maps prepared for physiochemical parameters that are measured in the field and studied with the geochemical data of bottom sediments to understand the suspended sediment concentration, turbidity, erosion, and coastline change in the study area.

## 5. Results

### 5.1. SSC mapping of NDSSI

Fig. 3a, the Normalized Difference Suspended Sediment Index (NDSSI) image of MSI shows the distribution of suspended sediments along the coast of the Al Arish – Al Ghariyah region. The image displays SSC values that range from –0.76 to 0.28, where –0.76 signifies high

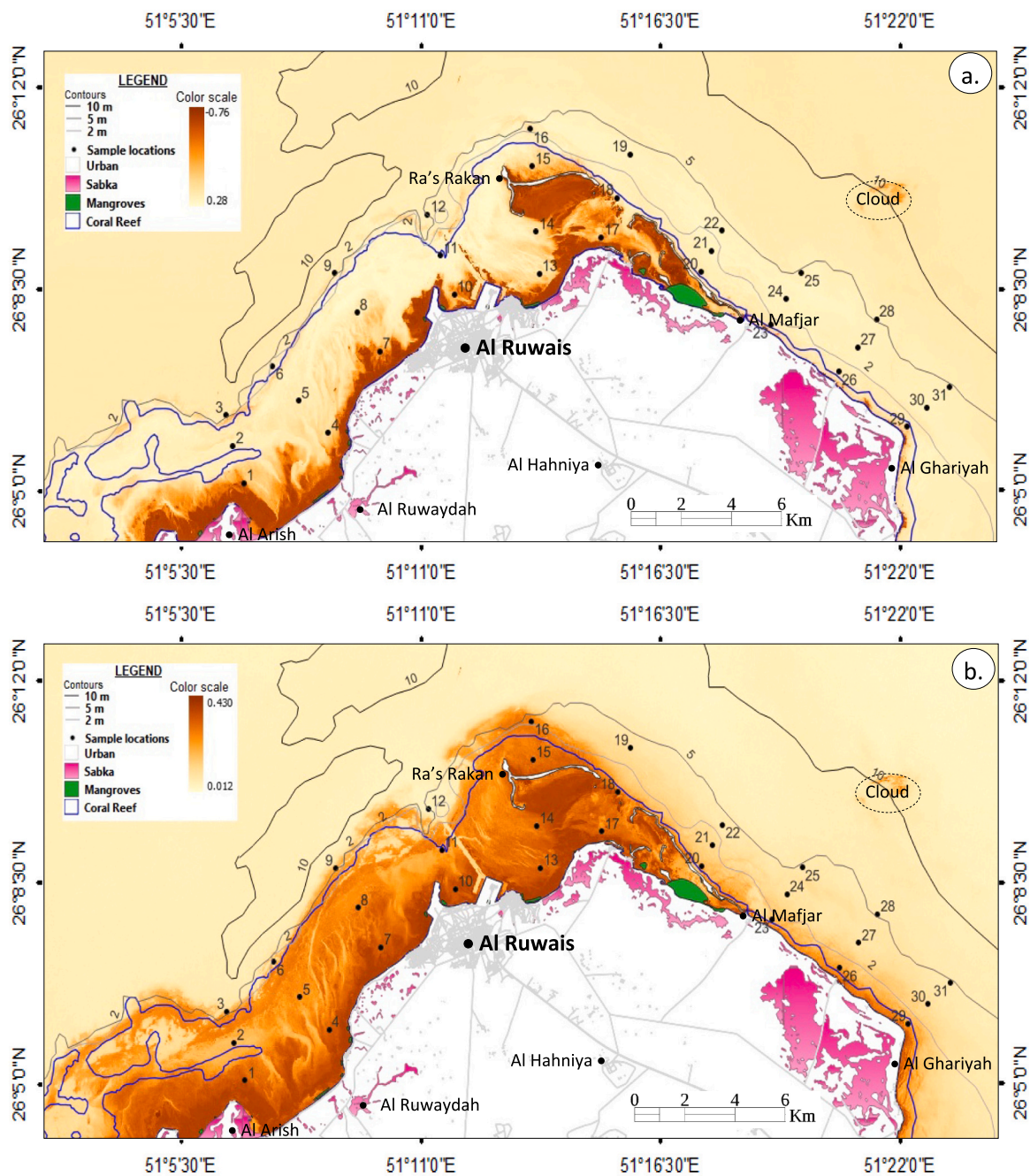


Fig. 3. a) Normalized Difference Suspended Sediment Index (NDSSI) image and b) Normalized Suspended Material Index (NSMI) image show TSS concentrations in Al Arish - Al Ghariyah coastal region, northern Qatar.

concentration and 0.28 represents the low concentration of sediments in the water. The area has high concentrations of suspended sediments exhibits dark brown, and the area with low concentrations of sediments appears light brown along the coastal region (Fig. 3a). The area that has no or very low concentration ( $>0.28$ ) exhibits a nearly white tone. The concentration of SSC is very high in the coastal water between Al Arish and Al Mafjar, and very low between Al Mafjar and Al Ghariyah. The variations in the concentration in the coasts may depends on the topography, waves and intertidal tidal effects and surface currents that prevailed along the coasts. The occurrence of more sediments is interpreted between Ra's Rakan Island and the coast where intertidal activity is high at the shallow depths of water. The distribution of SSC is relatively low in the area where corals occur (see boundary for coral reef,

Fig. 1) and the concentration of SSC is decreased from the coast towards offshore in the direction of NW. The distribution of sediments in the region occurs at the very shallow to shallow depths of water where the occurrence of clay and mud flats over the carbonate platform (Rajendran et al., 2022). The NDSSI uses blue and NIR bands and the results depend on the reflectivity of surface water and the concentration and distribution of suspended sediments. Xu et al. (2019) studied the MSI of Sentinel-2A and stated that the sensor detects reflectance of water to a maximum of 1.5 m depth from the surface of the Harsha Lake in the study about the mapping of Chl-a. They mentioned particularly that there is no backscattering of light in water beyond the depth. They compared the MSI results with the results of in-situ data obtained at a depth between 0.3 m and 0.5 m using a YSI sonde.

5.2. Suspended material mapping of NSMI

We mapped the suspended material, which may include suspended sediments with other materials, for example, dead algae, corals, sea grass, etc. using Normalized Suspended Material Index (NSMI) and MSI spectral bands, and the obtained result is given in Fig. 3b. The image shows values for suspended materials in the range from 0.012 (as clear water) to 0.430 (the presence of more suspended material). The occurrence and distribution of suspended materials (in dark brown to light brown) are very high on the coast between Al Arish and Al Mafjar and low between Al Mafjar and Al Ghariyah similar to the observation made using NDSSI. Hafeez et al. (2021) stated that the amounts of TSS are usually linearly related to turbidity, the NSMI index can be considered as an ideal indicator for tracking turbidity fronts in coastal areas. An

interpretation of the results of NSMI and NDSSI shows that the concentrations of the materials are very high when compared to the result of suspended sediments, which may be due to the occurrence of suspended materials in the region and the detection performance of the NSMI index which uses the bands of blue, green, and red. The water above 2 m appears in white due to the absence of such materials and the penetration of spectral information or the absorption of total light (Rajendran et al., 2021b; Xu et al., 2019). Rajendran et al. (2022) studied the area and showed the occurrence of mud and sand in the intertidal area situated over the carbonate platform. They also observed the presence of waves and tidal activities over the intertidal area. The NSMI results on the concentration of suspended material are comparable with the FCC image (Fig. 1 in Supplementary material).

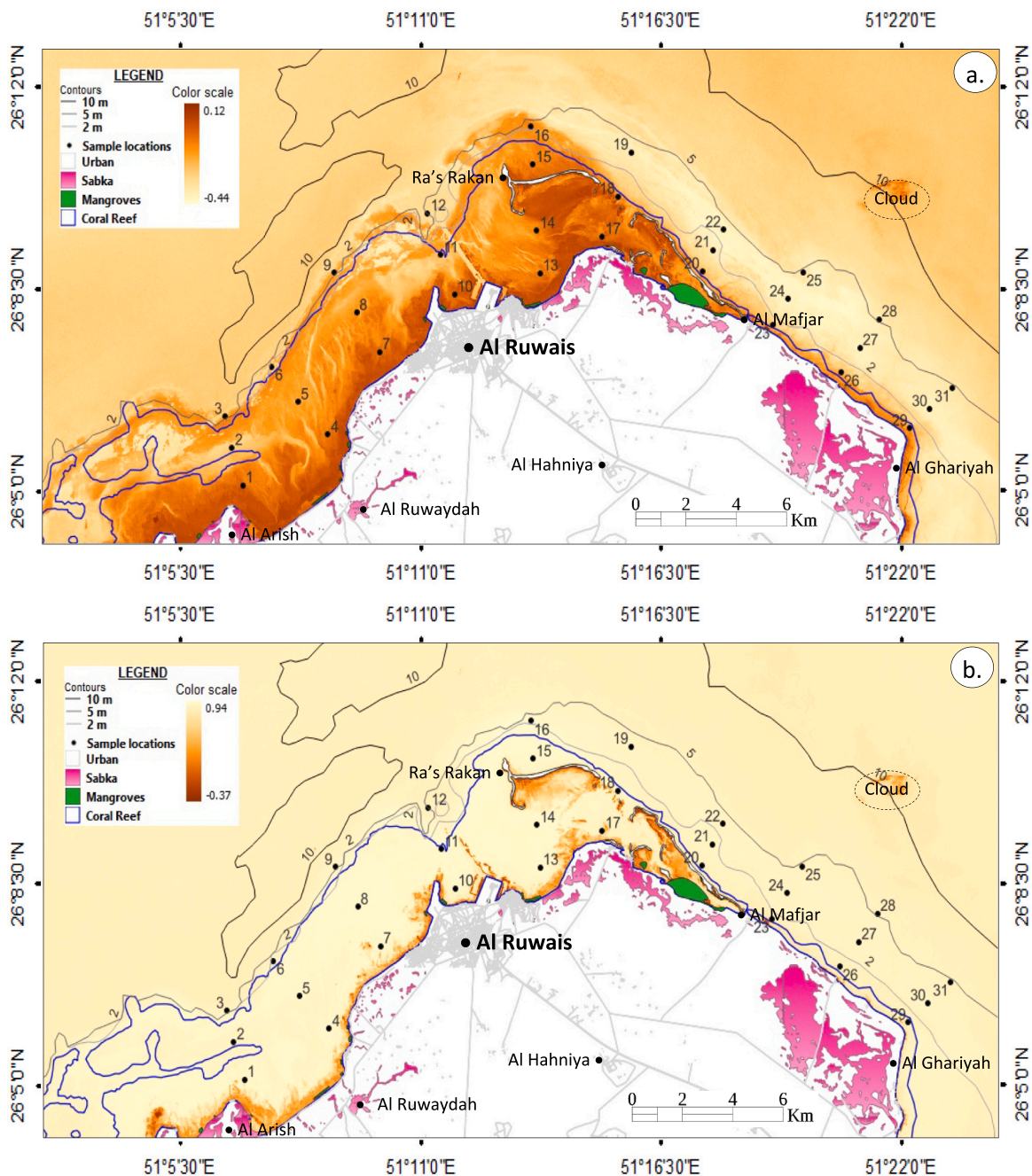


Fig. 4. a) Normalized Difference Turbidity Index (NDTI) image and b) Modified Normalized Difference Water Index (MNDWI) image show occurrences of turbidity and seawater in Al-Arish – Al Ghariyah coastal region, northern Qatar.

### 5.3. Turbidity mapping of NDTI

To understand further the concentration of suspended sediments and materials in the coastal region, we mapped the turbidity of water by the Normalized Difference Turbidity Index (NDTI) using the MSI data. The resulted image is given in Fig. 4a. The image shows the turbidity values range from  $-0.44$  (clear water) to  $0.12$  (high turbidity) for the occurrence and distribution of turbidity (in dark brown to light brown) in the water. The occurrence of very high turbidity is observed along the coast between Al Arish and Al Mafjar similar results that obtained on the mapping of suspended sediments and materials in the water of the region. The occurrence of low turbidity is interpreted in between the Al Mafjar and Al Ghariyah. The invaded water from the coast can be observed from a light tone and warp pattern in the direction of NW in the turbidity region. The turbidity could have been affected by the occurrence of waves, tides, and currents activities and the turbidity might have induced the occurrence of suspended materials and sediments in the region (Aboobacker et al., 2021; Rivers et al., 2020). The results can be used to integrate to study the waves and current direction in the region. The concentration of SSC depends on the presence of materials and the occurrence of turbidity and the NDTI results support and confirm the occurrence of suspended sediments and materials in the water of the study region. The study of turbidity invites us to study coastal erosion and deposition, and coastline changes in the region.

### 5.4. Discrimination of coastal water using MNDWI

The results obtained from NDSSI, NSMI, and NDTI are confirmed further by studying the extent of water along the coastline using MSI data by MNDWI. The delineation of the boundary of water along the coast is interpreted from the MNDWI image obtained using the green and SWIR bands (Fig. 4b). The image showed the presence of coastal water by bright pixels and the extent of water is well discriminated along the coast. The occurrence of clay and mud flats in between water and coastline that are exposed in the shore area is interpreted in light brown and fine texture on the coast between Al Arish and Al Mafjar. The deposits are more and wide along the coast when interpreted with the coast between Al Mafjar and Al Ghariyah where the sand deposits over the shore areas are thin. The MNDWI image discriminated the area of water extent and occurrence of sedimentary deposits. The results support and confirm the occurrence of turbid and the presence of suspended sediments and materials in the coastal water between Al Arish – Al Ghariyah.

### 5.5. Relationship of indices in mapping SSC

Several studies have demonstrated the relationship of remote sensing results with the field in-situ data and showed the capability of sensors and the used indices (Zhang et al., 2022; Li et al., 2022; Hossain et al., 2021, 2010; Lyburner et al., 2016; Binding et al., 2005). Saberioon et al. (2020) stated that the TSS was successfully predicted by the correlation of Sentinel-2A spectral bands, and water and TSS spectral indices. Zhang et al. (2022) estimated the SSC of the Yangtze Main Stream based on MSI data by developing a method to retrieve SSC that is suitable for rivers. They stated that the MSI data derived SSC provided good consistency with the SSCs measured from gauging stations at  $r^2 > 0.79$ . In this study, the relationship among the results obtained for SSC using NDSSI, suspended material using NSMI, and turbidity using NDTI were correlated with field measurement data to evaluate the indices and find the suitability of indices in the mapping of SSC. The image values of NDSSI, NSMI, and NDTI for the 31 locations were extracted and correlated with the in-situ data (Table 2 in Supplementary material) by statistical method. Table 1 provides the  $R^2$ , root means squared error (RMSE), slope,  $p$ , and intercept values of analysis to understand the relationships between the NDSSI and NSMI, NDSSI and NDTI, NSMI, and NDTI, and between the NDSSI, NSMI, and NDTI with the in-situ data. The fitting and accuracies can be interpreted from Fig. 3 in the

**Table 1**

Results of linear regression analysis performed using different indices and in-situ measured data for mapping of TSS in the Al Arish-Al Ghariyah coastal region.

Comparison	$R^2$	RMSE	Slope	Intercept	$p$
NDSSI vs NSMI	0.77	0.12	1.25	-0.81	<0.01
NDSSI vs NDTI	0.86	0.11	0.99	-0.34	<0.01
NSMI vs NDTI	0.95	0.03	0.73	0.36	<0.01
NDSSI vs In situ data	0.58	0.15	0.001	-0.62	0.57
NSMI vs In situ data	0.74	0.1	-0.001	0.2	0.89
MNDWI vs NDTI	0.79	0.05	0.04	0.89	0.64
MNDWI vs NSMI	0.76	0.04	0.12	0.86	0.28

### Supplementary material.

The regression analyses between different indices showed strong positive relationships between NSMI and NDTI ( $R^2 = 0.95$ ;  $RMSE = 0.03$ ), NDSSI vs NDTI where the NDTI had the strongest effect on NDSSI ( $R^2 = 0.86$ ;  $RMSE = 0.11$ ) (Fig. 3a-c in Supplementary material). NSMI was also able to predict NDSSI, however, not as effective as NDTI ( $\Delta R^2 = -0.09$ ;  $\Delta RMSE = +0.01$ ) (Table 1; Fig. 3a-c in Supplementary material). The interpretation suggests that the suspended sediments of NDSSI depend on the suspended material of NSMI and the turbidity of NDTI which are influenced very well by the occurrence of suspended sediments. Separate regression analyses of in-situ data with NDSSI and NSMI (Table 1; Fig. 3d and e in Supplementary material) showed much greater variance in the indices (NDSSI:  $R^2 = 0.58$ ;  $RMSE = 0.15$  and NSMI:  $R^2 = 0.74$ ;  $RMSE = 0.10$ ). The  $R^2$  value of NDSSI is lower than the value of NSMI and the variation may depend upon the spectral bands that are used among the indices, the time of sampling, and the number of waves, tides, and currents activities during sampling in the region. However, the relationship suggests that the NDSSI can be used very well to map SSC and that the blue and NIR spectral bands of the MSI are capable of providing more information about the SSC. In addition, the study of values of MNDWI with the suspended material (NSMI) and turbidity (NDTI) (Table 1; Fig. 3f and g in Supplementary material) shows no significant correlation between the material and turbidity in the water.

### 5.6. Validation and assessment

#### 5.6.1. Field studies

The results derived from the different indices were verified in the field by conducting several field trips and validated with the results obtained from the field studies. In the field, the northern part of Qatar is deposited mainly by the Dammam formation consisting of dolomite and limestone rocks (Emil et al., 2021; Al-Saad, 2005). The coastal region of the study area has gentle slopes, and the presence of accretion and erosional features are observed over the carbonate platform (Fig. 5a, b). The shore areas between Al Arish and Al Mafjar have a very gentle slope and occurred with very shallow depths of coastal water when studied with the coast between Al Mafjar and Al Ghariyah (Fig. 5c). The areas have wave and tide activities over silty sand flats and exposed to tidal flooding with the occurrence of silty sand deposits (Fig. 5d). The presence of clay and mud are observed along the coastline (Fig. 5c, d). The coastal water is turbid and muddy to a depth of up to 1 m and the occurrence of suspended sediments in water is well studied where waves and low tides and eddies are observed (Fig. 5c, e, f). The presence of channels developed by backwater erosional activity is observed (Fig. 5f). The area is occurred by mangroves (Fig. 5g; *Avicennia marina*) and stone barriers are developed for fish and crab catching (Fig. 5c). The silty sand flat exhibited ripples and occurred with shell fragments of invertebrates (Fig. 5h, i) on the beach and shore areas (Rajendran et al., 2022). Literature review shows that the region is occurred by degraded corals due to bleaching that occurred during summers (Riegl and Purkis, 2012).

Whereas, on the coast between Al Mafjar and Al Ghariyah (east coast region), the occurrence of thin sand deposits and massive carbonate

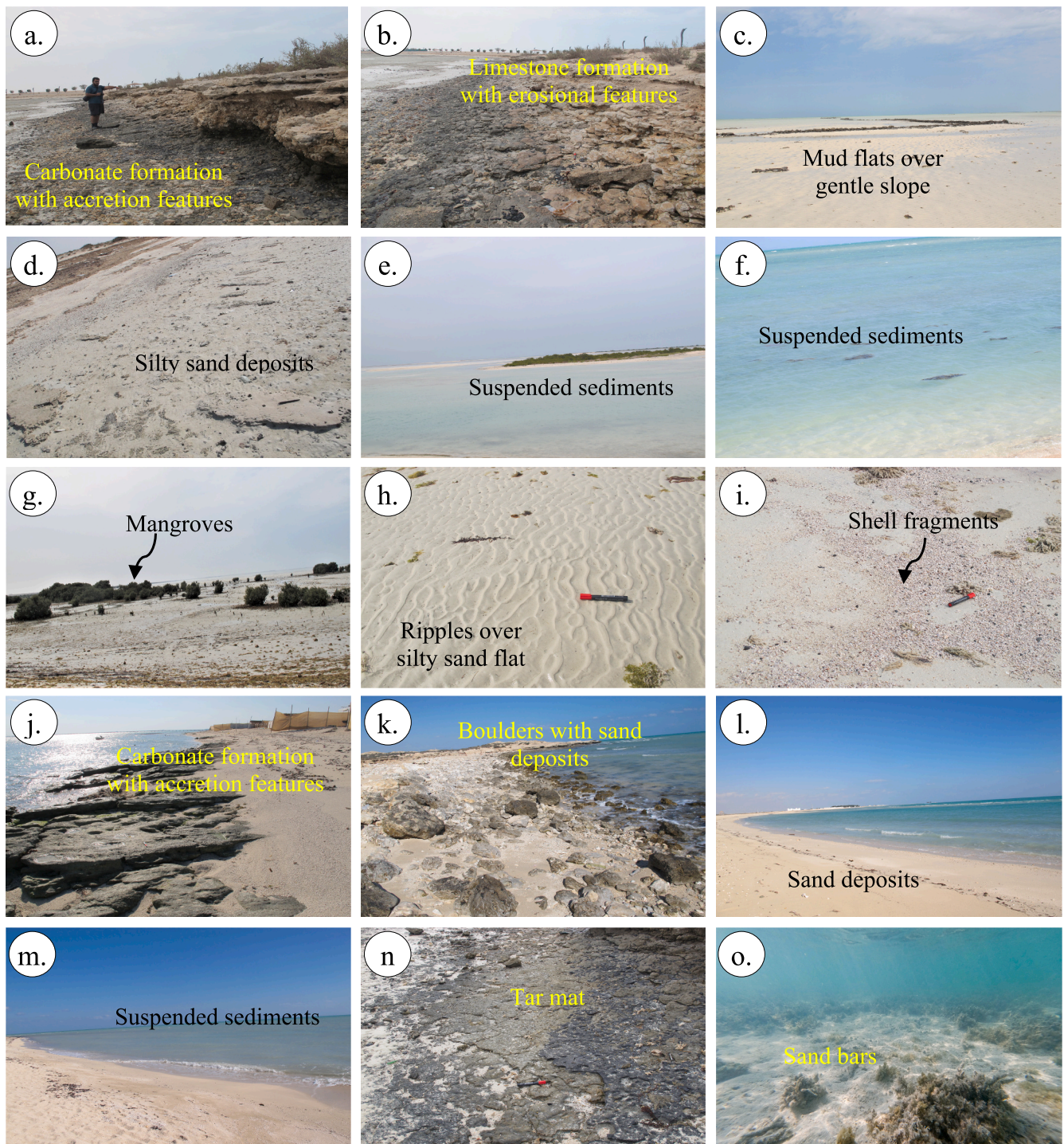


**Fig. 5.** Field photographs showing the occurrence of a) carbonate formation, b) accretion and erosional features, c) mud flats at very gentle slope, d) silty sand deposit, e) and f) suspended sediments, g) mangroves, h) ripple marks, and i) silty mud with shell fragments in the Al Arish - Al Mafjar coastal region, and the occurrence of j) massive carbonate rocks, k) boulders with sand deposits, l) sand deposits, m) suspended sediments in coastal water, n) tarmats over carbonate formation, and o) sand bars underwater in the Al Mafjar - Al Ghariyah coastal region.

formation along the coast is studied (Fig. 5j). The formation is well exposed at shallow depths and the occurrence of boulders and sediments are observed underwater (Fig. 5k). The sediments over the beaches and shore areas are mostly sand deposits mixed-up with shell fragments (Fig. 5l). The coast is not muddy, and the coastal water is relatively calm. The poor occurrence of suspended sediments in the water is observed when studied at the coast between Al Arish - Al Mafjar (Fig. 5m). The field study also showed the occurrence of tarmats over carbonate

formation (Fig. 5n) (Rajendran et al., 2021b). As well as, the growth of macroalgae over sand and carbonate formations is studied (Fig. 5j). The presence of sand bars formed by current activity is observed underwater (Fig. 5o) (Rajendran et al., 2022). The field photographs taken over the surface and bottom water at selected sample locations showed the presence of suspended sediments in the water between the Al Arish - Al Ghariyah region (Fig. 4 in the Supplementary material).

In addition, the measurements of temperature, Ec, pH, and total

dissolved solids (TDS) were carried out during fieldwork along the Al Arish - Al Ghariyah coast (Rajendran et al., 2022). Table 2 in Supplementary material provides the data of the parameters that were measured at the 31 sample locations (Fig. 1). The interpretations of data show the values of the minimum and maximum range of EC, pH, temperature, and TDS as 45,896 to 70,941  $\mu\text{S}/\text{cm}$ , 7.86 to 8.17, 19 to

29.9 °C, and 25,795 to 38,795 g/l respectively (Table 2 in Supplementary material). The study of the spatial distribution of these parameters shows that these parameters are high between Al Arish and Al Mafjar regions when studied between Al Mafjar and Al Ghariyah regions (Fig. 5a to d in Supplementary material). The high Ec, pH, and TDS of the region can be compared with the studies carried out in similar

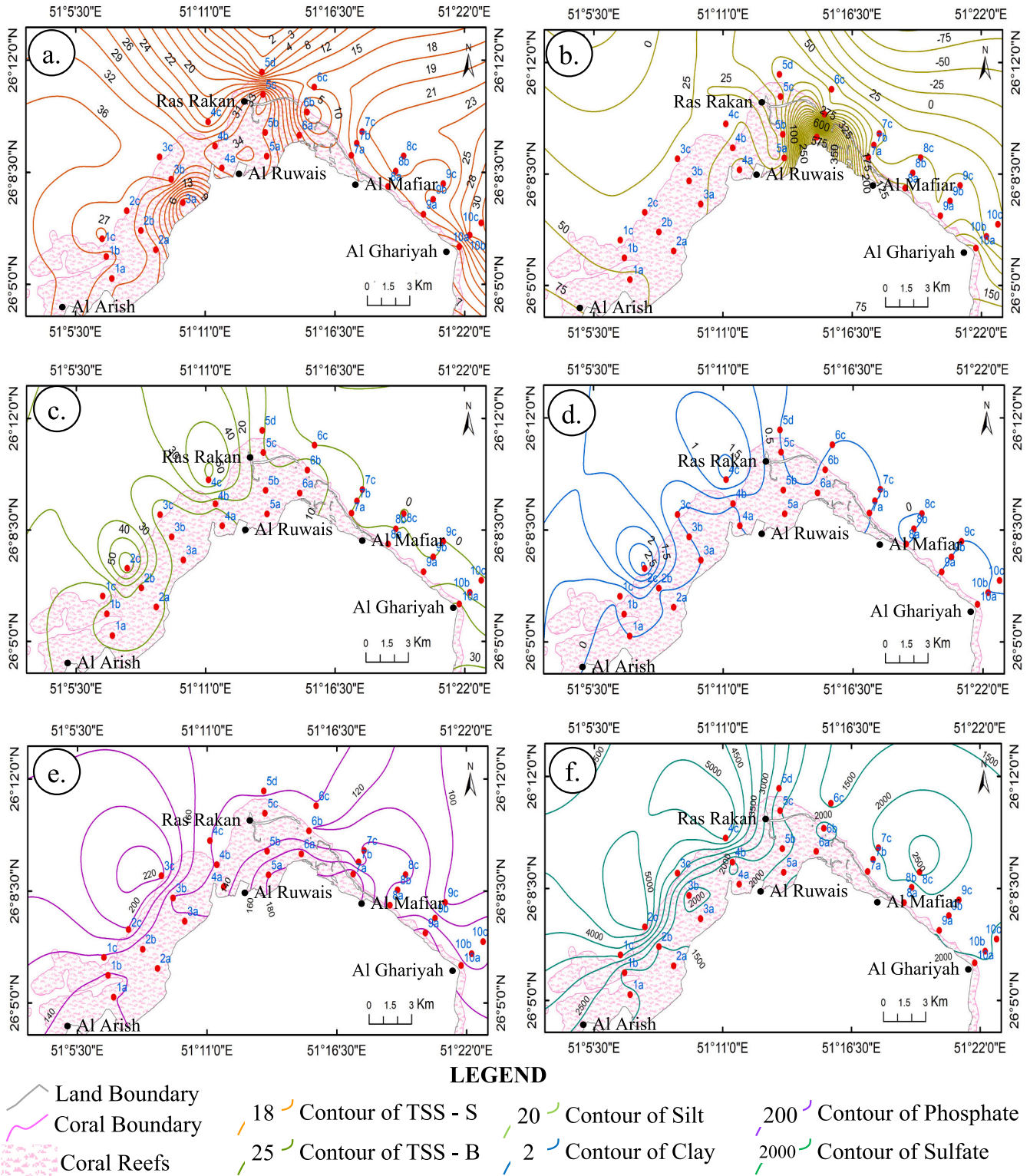


**Fig. 6.** Spatial distribution of total suspended sediments in (a) surface water (TSS-S in mg/l), (b) bottom water (TSS-B in mg/l), and distribution of (c) silt (in %), (d) clay (in %), (e) phosphate (in mg/Kg) and (f) sulfate (in mg/Kg) contents in bottom sediments in between Al Arish and Al Ghariyah region of northern Qatar.

regions by Ibrahim et al. (2020), Youssef et al. (2015), and Kampf and Sadrinasab (2006).

5.6.2. Laboratory studies

Surface and bottom water samples collected from the field were analyzed for TSS to understand the SSC. Table 2 in the Supplementary material provides the concentration of TSS in the coastal water along the Al Arish – Al Ghariyah coast. It shows the minimum and maximum concentrations as 28.04 and 90.33 mg/l in the surface water and about 30 and 678.11 mg/l in the bottom water respectively. The spatial distribution maps prepared for the concentration of TSS in the surface and bottom waters (Fig. 6a and b) show the existence of a high concentration of TSS between Al Arish and Al Mafjar and very high in between Ra’s Rakan and Al Ruwais in the bottom water when studied with the coast between Al Mafjar and Al Ghariyah as interpreted from the NDSSI and NSMI images (Fig. 3a and b). The sediments are distributed in the shallow water and the region where the corals have occurred. The occurrence of waves, tides, and currents in the region could have

developed turbidity over the carbonate platform which has gentle topography and caused the distribution of sediments consisting of silt, clay, sand, and other materials in the water (Aboobacker et al., 2021; Rivers et al., 2020). The measured TSS values from the water confirmed the presence of sediments and validated the results of NDSSI and NSMI.

In addition, the bottom sediments collected from the locations were analyzed for grain sizes and the results are given in Table 3 in Supplementary material. It shows that the samples predominantly occurred with sand and silt (Purkis et al., 2017; Al-Ghadban and El-Sammak, 2005). The occurrence of silty sand is observed along the coast of Al Arish - Al Mafjar and the distribution of sand is interpreted between Al Mafjar and Al Ghariyah (Table 3 in Supplementary material). An integrated study of the results of NDSSI, NSMI, and NDTI with the spatial maps prepared for the distribution of silt and clay of the region (Fig. 6c and d) confirms the presence of more suspended sediments on the coast between Al Arish and Al Mafjar when studied with the coast between Al Mafjar and Al Ghariyah. In addition, the analysis of sediment samples for the concentration of carbonate (CO<sub>3</sub>), silica (Si), phosphate (PO<sub>4</sub>),

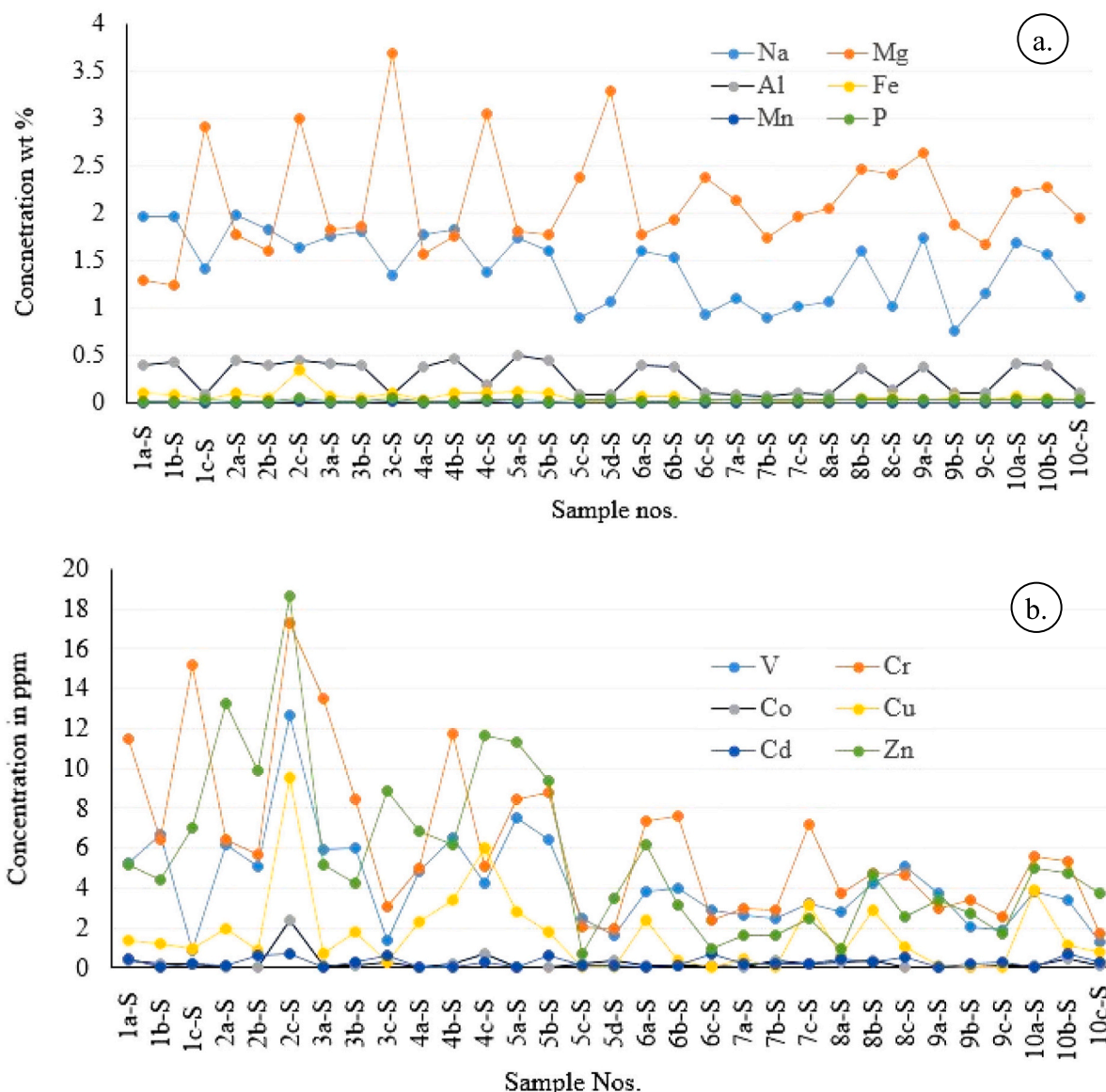


Fig. 7. Variation plots showing the distribution of selected a) major and b) trace elements concentrations in the bottom sediments of Al Arish – Al Ghariyah coastal region of northern Qatar.

sulfate (SO<sub>4</sub>), chloride (Cl), and fluoride (F) in the laboratory shows that the samples have a high concentration of carbonate (Table 3 in Supplementary material) and reflects the occurrence of carbonate rocks in the region (Purkis et al., 2017). The minimum and maximum concentrations of CO<sub>3</sub>, Si, PO<sub>4</sub>, SO<sub>4</sub>, F, and Cl elements are 64.09 to 89.34 %, 8.21 to 47.73, 100.8 to 223.81, 1416.25 to 5230.03, 4.16 to 6.35 mg/Kg and 5830.94 to 15,301.34 ppm/Kg respectively. The occurrence of high concentrations of sulfate and phosphate in the coastal region (Fig. 6e and f) is due to the input of evaporites that occurred in the sabkhas situated along the coast, and shells and skeletons of dead life found on the shore and bottom areas. These concentrations are confirmed further by the study of the occurrence of minerals in the samples. The analysis of minerals in the sediment samples by X-ray Diffraction method showed the concentration of elements by the presence of aragonite, calcite, dolomite, and quartz minerals in the samples (Fig. 6 in Supplementary material).

Table 4 in the Supplementary material shows the major and trace element concentrations of bottom sediments. It shows that the sediments have a high concentration of calcium and magnesium. The sediments have elements enrichment in the decreasing order of Ca > Mg > Na > Al > Fe > Mn > P and the maximum and minimum values of Ca, Mg, Na, Al, and Fe are 41.2 and 32.56, 3.68, and 1.23, 1.98 and 0.74, 0.49 and 0.07, 0.33 and 0.01 % respectively (Fig. 7a; Table 4 in Supplementary material) (Mora et al., 2004; Basaham and El-Sayed, 1998). The enrichment of elements in the samples is due to the input of terrigenous and or weathered contents of limestone and dolomite formations that occurred in the region (Basaham and El-Sayed, 1998). The occurrence of low concentrations of Fe, Al, Mn, and P is studied in the sediments. The low concentrations of such elements are due to the presence of clay or mud derived from shale formations that are interbedded in the carbonate formations (Al-Saad, 2005). In addition, the sediments have a high concentration of bromine and strontium (maximum of 12,835 and 7768 ppm respectively) which may be due to the interaction of seawater (Rivers et al., 2019). The other trace elements such as Ni, Ba, Zn, Cr, V, and Cu showed the maximum and minimum concentrations of 77.7 and 1.69, 75.36 and 9.43, 18.62 and 0.71, 17.31 and 1.72, 12.69 and 0.9, and 9.53 and 0.11 ppm respectively (Fig. 7b; Table 4 in Supplementary material). Such concentrations are due to the input of terrigenous contents in the sediments (Youssef et al., 2015; Janadeleh et al., 2018; Basaham and El-Sayed, 1998). The bottom sediments also showed significant concentrations of Co and Cd, which may be due to the bioaccumulation in the sediments (Mora et al., 2004).

## 6. Discussion

Study of SSC is important to understand water quality that plays a major role in the biological processes in the coastal waters. SSC is an indicator of the biophysical status of coastal waters and requires continued monitoring. It is an optically active component enabling measurements by remote sensing. Available conventional methods (including in-situ monitoring) to map and monitor suspended sediment concentration have revealed that they are difficult due to time and space limitations. In this context, the satellite-derived SSC overcomes these problems since in-situ measurements of SSC are laborious, costly, and spatially discontinuous. Thus, this study discussed the conventional methods including laboratory analysis, and optical and acoustic methods, and emphasized the importance and uses of different sensors and spectral band indices in mapping SSC in river, coastal, delta, and estuaries water. The study briefed the application of the data of the airborne platforms (AVIRIS, CASI) and the satellites such as the SeaWiFS, MERIS, MODIS, SPOT, Landsat series, GeoEye-1, WorldView-3 and Sentinel-2 and also the indices including the NDSSI, NSMI, NDTI, and MNDWI. Since no study was carried out to assess the suspended sediments of the coastal waters in the Gulf, which is situated in an arid environment using satellite data, this study aimed to use the MSI spectral bands of Sentinel-2 to assess the occurrence and spatial distribution

of SSC in parts of the northern Qatar. Sentinel-2 satellites offer higher spatial, spectral, and temporal resolution images at free of cost for monitoring the water quality of coastal waters. The MSI of the satellites has four visible bands and three NIR bands, making the instrument more effective for the measurement of SSC. The study showed the spectral absorptions of sediments and gulf waters among the bands of MSI by reviewing the published literature (Peterson et al., 2018; Wang and Lu, 2010; Lodhi et al., 1997; Chen et al., 1991) and highlighted the significance of blue and NIR bands in the mapping of SSC. Subsequently, the study used spectral band-derived indices such as NDSSI and NSMI and mapped the concentration of suspended sediments and materials that occurred in the study region. Mapping of suspended sediments using the NDSSI showed the presence of very high SSC along the coast between Al Arish and Al Mafjar and low in between Al Mafjar and Al Ghariyah region. The spatial distribution maps derived from the MSI data having 10 m spatial resolution showed well the SSC where the SSC was relatively high. The occurrence and distribution of SSC were studied with the results of NSMI and NDTI indices, which supported the distribution of SSC. The area of extent of coastal waters was well distinguished using MNDWI to support further the results of NDSSI and NSMI. The relationship among the NDSSI, NSMI, and NDTI with in-situ measurements were studied and demonstrated. The presence of the strongest relationship was between NSMI and NDTI ( $R^2 = 0.95$ ), followed by NDSSI and NDTI ( $R^2 = 0.86$ ) was analyzed. The indices derived from MSI bands were successful in showing areas of SSC concentration for assessing their distribution along the coast of Al Arish - Al Ghariyah.

The results obtained from MSI data were validated through a combination of field studies and laboratory analyses. In the field, Al Arish and Al Mafjar regions showed a very gentle slope, which had deposits of silty sand, clay, and mud. Whereas, the occurrence of sand deposits and rocky boulders was studied along the coast between Al Mafjar and Al Ghariyah. The field study of the coasts can be studied with the study of the coast of Ra's Rakan Island of the study region carried out by Rajendran et al. (2021a, 2021b). The study described that the coast of the island is deposited by sandy soil, and the beaches are covered with coarse sand, clayey sand, shells, and dead algae as observed in the study region. The researchers stated that the sandy banks are extended to a few meters offshore and that the inner ramp of the island is deposited by clayey sand and accumulation of shells of Turrilites and dead algae. In addition, they also studied the occurrence of sand and mud deposits over mud flats over the carbonate platform at shallow depths in the study region (Rajendran et al., 2022). They have also observed the presence of corals and the erosion and depositional activities in the intertidal area. The sediment characters and presence of extensive dead corals, fossils, algae, etc. in northern Qatar are also studied by Bouwmeester et al. (2022), Burt et al. (2019, 2016), and Purkis et al. (2017).

The field study also discussed the physical parameters such as the temperature Ec, pH, and TDS of the region. The measurement of TSS over surface water and in bottom water at 31 sites showed the presence of TSS concentrations from 28.04 to 90.33 mg/l in the surface water and about 30 to 678.11 mg/l at the bottom water. The occurrence of suspended sediments in the surface water reached a minimum of 28.36 mg/l and a maximum of 678.1 mg/l at the bottom water that can be compared with the results of NDSSI and NSMI. However, the distribution tendency of suspended sediments is caused by the presence of turbidity, which is induced by surface winds and waves, currents, and tides that occur in the region. Al-Hulail and Neelamani (2011) studied the variation of TSS in the seawater samples in a similar region of Khor Sabiya Inlet of Kuwait. They stated that the average TSS values at the seabed, mid-depth, and surface in shallow water inlet are 289.75 mg/l, 278.63 mg/l, and 258.38 mg/l respectively. The TSS values of the study region are low when compared to the TSS values of the water of the inlet, which may be due to the gentle slope, nature of sediments, and conditions of waves and tides that prevailed at the time of samples collections. As well as, the bottom sediments of the region were studied for grain size distributions, which showed the occurrence of a high amount of silt and

sand in the samples. The sediment characters can be well interpreted with the field study of Purkis et al. (2017). Moreover, the analyses of carbonate, silica, phosphate, sulfate, chloride, and fluoride in the samples showed the presence of high contents of carbonate and reflected the occurrence of carbonate formation in the region. The concentration of sulfate and phosphate suggested that these could have been derived from the evaporites that occurred in the sabkhas situated along the coast, and shells and skeletons that were found in the shore areas. The samples analyzed for minerals by XRD analyses confirmed the presence of the aragonite, calcite, and dolomite minerals and showed the mineral's character of sediments, and supported the concentration of elements. This study showed that the sediments were characterized by the inputs of terrigenous and or carbonate formations.

As well as, the analyses of major and trace elements of sediment samples presented the enrichment in the decreasing order of  $Ca > Mg > Na > Al > Fe > Mn > P$  elements. The presence of a high concentration of Ca and Mg suggested the presence of carbonate minerals in the samples and the low concentrations of Al, Fe, Mn, and P were due to the presence of silts in the samples that derived from the shale formations (interbedded in carbonate formations) of the region. The study of the concentration of trace elements showed a very high concentration of bromine and strontium (maximum of 12,835 and 7768 ppm respectively) in the sediments. The other trace elements such as Ni, Ba, Zn, Cr, V, and Cu showed the presence of significant concentrations due to the input from terrigenous sediments. The distribution of such trace elements can be studied with the distribution of the heavy metals in the samples that were collected from a similar coastal region of Abu Dhabi (UAE) (Al Rashdi et al., 2015). Overall, it can be summarized that the use of MSI spectral bands and indices employed in this study showed best the concentration of suspended sediments along the coast of Al Arish – Al Ghariyah and the field and laboratory studies validated the results of the satellite data.

## 7. Conclusions

This study mapped the distribution of suspended sediments in the Arabian Gulf water of an arid region using higher spatial resolution (10 m) spectral bands of MSI of Sentinel-2A and indices such as NDSSI and NSMI and studied with NDTI and MNDWI. The mapping of SSC along the coast of the Al Arish - Al Ghariyah region of Qatar showed clearly the occurrence of suspended sediments. The concentration of SSC is very high on the coast of Al Arish - Al Mafjar and low between Al Mafjar and Al Ghariyah. The results are supported by studies on the mapping of suspended materials and turbidity of the region. The relationship among the results of NDSSI, NSMI, and NDTI was correlated with field in-situ data and determined the capability of indices to map SSC. The spatial distribution of TSS over surface water and bottom water was studied in the field and the concentration of TSS at 31 locations was measured and studied. In addition, the distribution of sediments is studied in the field and verified. The grain size, distribution of clay, silt, and sand, identification of minerals, and concentration of major and trace elements of bottom sediments were studied and used to validate the remote sensing results in the mapping of the SSC of Gulf water. The study showed that the sediments predominantly occurred with sand and silt consisting of aragonite, calcite, and dolomite minerals. The sediments have elements enrichment in the decreasing order of  $Ca > Mg > Na > Al > Fe > Mn > P$ . The concentration of trace elements Ni, Ba, Zn, Cr, V, and Cu are discussed. The study showed that the enrichments are due to the input of terrigenous contents that are derived from the shale and carbonate formations and bioaccumulation in the sediments. The study demonstrated the potential use of MSI spectral bands and the capability of indices to map the concentration of suspended sediments of gulf water. The data and methods were found reliable and inexpensive to study similar regions elsewhere in the world.

## CRedit authorship contribution statement

**Sankaran Rajendran:** Conceptualization, Methodology, Data Analysis and Interpretation and Writing Original draft. **Jassim A. Al Khayat:** Field Investigation and Reviewing. **Aravinth J:** Data analysis and Reviewing. **Mark Edward Chatting:** Field samples collection, data analysis and Reviewing. **Fadhil N. Sadooni:** Investigation, Visualization and Reviewing. **Hamad Al-Saad Al-Kuwari:** Investigation, Visualization and Reviewing.

## Declaration of competing interest

The authors declare that they have no known competing financial interests or personal relationships that could have appeared to influence the work reported in this paper.

## Data availability

Data will be made available on request.

## Acknowledgments

Qatar National Library funded the publication of this article. This study is supported by Qatar University Grant no. QUEX-ESC-QAFCO-20/21-1. The Copernicus, European Space Agency is thanked for sharing the Sentinel-2 data through the sentinel open access hub (<https://sentinel.esa.int/web/sentinel/sentinel-data-access>). Mr. Fahad Syed Asim, Mr. Faisal Muthar Al-Quaiti, and Mr. Reyniel M. Gasang are thanked for their support in the fieldwork. The sediment samples for different analyses are organized by Ms. Thoraya Haidar S A Alyafei. The grain size analysis is carried out by Ms. Amal Ahmed Ibrahim Ismail. Mr. Abdulla Al Ashraf, CAM is thanked for the XRD analysis of samples. Mr. Caesar Flonasca Sorino, Mr. Hamood Abdulla Alsaadi, and Ms. Marwa Mustufa Al-Azhari have analyzed major and trace element concentrations of sediment samples. The authors are thankful to Prof. Wei Ouyang, the Associate Editor and anonymous reviewers of the journal for the valuable reviews, providing comments and suggestions that have helped to present the work lucidly.

## Appendix A. Supplementary data

Supplementary data to this article can be found online at <https://doi.org/10.1016/j.scitotenv.2023.166875>.

## References

- Aboobacker, V.M., Vethamony, P., Rashmi, R., 2011. "Shamal" swells in the Arabian Sea and their influence along the west coast of India. *Geophys. Res. Lett.* 38, L03608. <https://doi.org/10.1029/2010GL045736>.
- Aboobacker, V.M., Samiksha, S.V., Veerasingam, S., Al-Ansari, E.M.A.S., Vethamony, P., 2021. Role of shamal and easterly winds on the wave characteristics off Qatar, central Arabian gulf. *Ocean Eng.* 236, 109457 <https://doi.org/10.1016/j.oceaneng.2021.109457>.
- Al Rashdi, S., Arbi, A.A., Howari, F.M., Siad, A., 2015. Distribution of heavy metals in the coastal area of Abu Dhabi in the United Arab Emirates. *Mar. Pollut. Bull.* 97, 494–498. <https://doi.org/10.1016/j.marpolbul.2015.05.052>.
- Al Senafi, F., Anis, A., 2015. Shamals and climate variability in the Northern Arabian/Persian Gulf from 1973 to 2012. *Int. J. Climatol.* 35, 4509–4528. <https://doi.org/10.1002/joc.4302>.
- Al-Ghadban, A.N., El-Sammak, A., 2005. Sources, distribution and composition of the suspended sediments, Kuwait Bay, Northern Arabian Gulf. *J. Arid Environ.* 60 (4), 647–661. <https://doi.org/10.1016/j.jaridenv.2004.07.017>.
- Al-Hulail, F., Neelamani, S., 2011. The variation of total suspended sediments due to the change in sea water depth, tidal phase and elevation of sea water sample collection in Khor Sabiya Inlet of the Arabian Gulf, Kuwait. In: Micallef, A. (Ed.), *MCCR3-2010 Conference Proceedings, Journal of Coastal Research, Special Issue, vol. No. 61*. Grosseto, Tuscany, Italy, pp. 369–374 (ISSN 0749-0208).
- Al-Saad, H., 2005. Lithostratigraphy of the Middle Eocene Dammam Formation in Qatar, Arabian Gulf: effects of sea-level fluctuations along a tidal environment. *J. Asian Earth Sci.* 25, 781–789. <https://doi.org/10.1016/j.jseae.2004.07.009>.
- Al-Yousef, M., 2003. Mineralogy, Geochemistry and Origin of Quaternary Sabkhas in the Qatar Peninsula, Arabian Gulf (Unpublished thesis). University of Southhaption, UK.

- Arisanty, D., Nur Saputra, A., 2017. Remote sensing studies of suspended sediment concentration variation in Barito Delta. In: IOP Conference Series: Earth and Environmental Science, 98. <https://doi.org/10.1088/1755-1315/98/1/012058> (012058).
- Balasubramanian, S.V., Pahlevan, N., Smith, B., Binding, C., Schalles, J., Loisel, H., Gurlin, D., Greb, S., Alikas, K., Randa, M., Bunkei, M., Moses, W., Nguyễn, H., Lehmann, M.K., O'Donnell, D., Ondrusek, M., Han, T.H., Fichot, C.G., Moore, T., Boss, E., 2020. Robust algorithm for estimating total suspended solids (TSS) in inland and nearshore coastal waters. *Remote Sens. Environ.* 246, 111768 <https://doi.org/10.1016/j.rse.2020.111768>.
- Basaham, A.S., El-Sayed, M.A., 1998. Distribution and phase association of some major and trace elements in the Arabian Gulf sediments. *Estuar. Coast. Shelf Sci.* 46 (2), 185–194. <https://doi.org/10.1006/ecss.1997.0278>.
- Bid, S., Siddique, G., 2019. Identification of seasonal variation of water turbidity using NDTI method in Panchet Hill Dam, India. *Model. Earth Syst. Environ.* 5, 1179–1200. <https://doi.org/10.1007/s40808-019-00609-8>.
- Binding, C.E., Bowers, D.G., Mitchelson-Jacob, E.G., 2005. Estimating suspended sediment concentrations from ocean color measurements in moderately turbid waters: the impact of variable particle scattering properties. *Remote Sens. Environ.* 94 (3), 373–383. <https://doi.org/10.1016/j.rse.2004.11.002>.
- Bouwmeester, J., Ben-Hamadou, R., Range, P., Al Jamali, F., Burt, J.A., 2022. Spatial patterns of reef fishes and corals in the thermally extreme waters of Qatar. *Front. Mar. Sci.* 9, 989841 <https://doi.org/10.3389/fmars.2022.989841>.
- Burt, J.A., Smith, E.G., Warren, C., Dupont, J., 2016. An assessment of Qatar's coral communities in a regional context. *Mar. Pollut. Bull.* 105 (2), 473–479. <https://doi.org/10.1016/j.marpolbul.2015.09.025>.
- Burt, J.A., Paparella, F., Al-Mansoori, N., Al-Mansoori, A., Al-Jailani, H., 2019. Causes and consequences of the 2017 coral bleaching event in the southern Persian/Arabian Gulf. *Coral Reefs* 38 (4), 567–589. <https://doi.org/10.1007/s00338-019-01767-y>.
- Caballero, I., Steinmetz, F., Navarro, G., 2018. Evaluation of the first year of operational sentinel-2a data for retrieval of suspended solids in medium- to high-turbidity waters. *Remote Sens.* 10 <https://doi.org/10.3390/rs10070982>.
- Cavalcante, G.H., Feary, D.A., Burt, J.A., 2016. The influence of extreme winds on coastal oceanography and its implications for coral population connectivity in the southern Arabian Gulf. *Mar. Pollut. Bull.* 105, 489–497. <https://doi.org/10.1016/j.marpolbul.2015.10.031>.
- Chalov, S.R., Bazilova, V.O., Tarasov, M.K., 2017. Suspended sediment balance in Selenka delta at the late XX–early XXI century: simulation by LANDSAT satellite images. *Water Res.* 44, 463–470. <https://doi.org/10.1134/S0097807817030071>.
- Chalov, S.R., Potemkina, T.G., Pashkina, M.P., Kasimov, N.S., 2019. Long-term changes of the budget of suspended sediment in the deltas of the tributaries of Lake Baikal. *Meteorol. Hydrol.* 10, 50–59 (In Russian).
- Chalov, S., Prokopenko, K., Habel, M., 2021. North to South variations in the suspended sediment transport budget within Large Siberian River Deltas revealed by remote sensing data. *Remote Sens.* 13, 4549. <https://doi.org/10.3390/rs13224549>.
- Chen, Z., Hanson, J.D., Curran, P.J., 1991. The form of the relationship between suspended sediment concentration and spectral reflectance: its implications for the use of Daedalus 1268 data. *Int. J. Remote Sens.* 12 (1), 215–222. <https://doi.org/10.1080/01431169108929647>.
- Clevers, J.G.P.W., Gitelson, A.A., 2013. Remote estimation of crop and grass chlorophyll and nitrogen 682 content using red-edge bands on Sentinel-2 and -3. *Int. J. Appl. Earth Obs. Geoinf.* 23, 344–351. <https://doi.org/10.1016/j.jag.2012.10.008>.
- Do, H.X., Westra, S., Leonard, M., 2017. A global-scale investigation of trends in annual maximum streamflow. *J. Hydrol.* 552, 28–43. <https://doi.org/10.1016/j.jhydrol.2017.06.015>.
- Dogliotti, A.I., Ruddick, K.G., Nechad, B., Doxaran, D., Knaeps, E., 2015. A single algorithm to retrieve turbidity from remotely-sensed data in all coastal and estuarine waters. *Remote Sens. Environ.* 156, 157–168. <https://doi.org/10.1016/j.rse.2014.09.020>.
- Dörnhöfer, K., Klingner, P., Heege, T., Oppelt, N., 2018. Multi-sensor satellite and in situ monitoring of phytoplankton development in a eutrophic-mesotrophic lake. *Sci. Total Environ.* 612, 1200–1214. <https://doi.org/10.1016/j.scitotenv.2017.08.219>.
- Doxaran, D., Froidefond, J.M., Castaing, P., Babin, M., 2009. Dynamics of the turbidity maximum zone in a macrotidal estuary (the Gironde, France): observations from field and MODIS satellite data. *Estuar. Coast. Shelf Sci.* 81 (3), 321–332. <https://doi.org/10.1016/j.ecss.2008.11.013>.
- Drusch, M., Bello, D.U., Carlier, S., Colin, O., Fernandez, V., Gascon, F., Hoersch, B., Isola, C., Laberinti, P., Martimort, P., Meygret, A., Spoto, F., Sy, O., Marchese, F., Bargellini, P., 2012. Sentinel-2: ESA's optical high-resolution mission for GMES operational services. *Remote Sens. Environ.* 120, 25–36. <https://doi.org/10.1016/j.rse.2011.11.026>.
- Elhag, M., Gitas, I., Othman, A., Bahrawi, J., Gikas, P., 2019. Assessment of water quality parameters using temporal remote sensing spectral reflectance in arid environments, Saudi Arabia. *Water* 11, 556. <https://doi.org/10.3390/w11030556>.
- El-Sabh, M.I., Murty, T.S., 1989. Storm surges in the Arabian Gulf. *Nat. Hazards* 1, 371–385. <https://doi.org/10.1007/BF00134834>.
- Emil, M.K., Sultan, M., Alakhras, K., Sataer, G., Gozi, S., Al-Marri, M., Gebremichael, E., 2021. Countrywide monitoring of ground deformation using InSAR time series: a case study from Qatar. *Remote Sens.* 13, 702. <https://doi.org/10.3390/rs13040702>.
- ESA, 2015. European Space Agency. Sentinel-2 User Handbook. ESA Standard Document. European Space Agency, Paris, France.
- Feyisa, G.L., Meilby, H., Fensholt, R., Proud, S.R., 2014. Automated Water Extraction Index: a new technique for surface water mapping using Landsat imagery. *Remote Sens. Environ.* 140, 23–35. <https://doi.org/10.1016/j.rse.2013.08.029>.
- Frayne, C., 2010. 4.27 - Environmental Modification for Cooling, Heating and Potable Water Systems. Reference Module in Materials Science and Materials Engineering, Editor(s): Bob Cottis, Michael Graham, Robert Lindsay, Stuart Lyon, Tony Richardson, David Scantlebury, Howard Stott. Shreir's Corrosion, 4, pp. 2930–2970. <https://doi.org/10.1016/B978-044452787-5.00161-X>.
- Garg, V., Aggarwal, S.P., Chauhan, P., 2020. Changes in turbidity along Ganga River using Sentinel-2 satellite data during lockdown associated with COVID-19. *Geomat. Nat. Haz. Risk* 11 (1), 1175–1195. <https://doi.org/10.1080/19475705.2020.1782482>.
- Gernez, P., Lafon, V., Lerouxel, A., Curti, C., Lubac, B., Cerisier, S., Barille, L., 2015. Toward Sentinel 2 high resolution remote sensing of suspended particulate matter in very turbid waters: SPOT 4 (Take5) experiment in the Loire and Gironde estuaries. *Remote Sens.* 7 (8), 9507–9528. <https://doi.org/10.3390/rs70809507>.
- Gohin, F., der Zande, D.V., Tilstone, G., Eleveid, M.A., Lefebvre, A., Andrieux-Loyer, F., Blauw, A.N., Bryre, P., Devreker, D., Garnesson, P., Farias, T.H., Lamaury, Y., Lampert, L., Lavigne, H., Menet-Nedelec, F., Pardo, S., Saulquin, B., 2019. Twenty years of satellite and in situ observations of surface chlorophyll-a from the northern Bay of Biscay to the eastern English Channel. Is the water quality improving? *Remote Sens. Environ.* 233, 111343 <https://doi.org/10.1016/j.rse.2019.11.1343>.
- Govinda Rao, P., Al-Sulaiti, M., Al-Mulla, A.H., 2001. Winter Shamals in Qatar, Arabian Gulf. *Weather* 56, 444–451. <https://doi.org/10.1002/j.1477-8696.2001.tb06528.x>.
- Gray, J.R., Glysson, G.D., Turcios, L.M., Schwarz, G.E., 2000. Comparability and reliability of total suspended solids and suspended-sediment concentration data. In: USGS Water-Resources Investigations Rep. No. 2000-4191. <https://doi.org/10.3133/wri004191>.
- Guerrero, M., Rüther, N., Haun, S., Baranya, S., 2017. A combined use of acoustic and optical devices to investigate suspended sediment in rivers. *Adv. Water Resour.* 102, 1–12. <https://doi.org/10.1016/j.advwatres.2017.01.008>.
- Guimares, T.T., Veronez, M.R., Koste, E.C., Souza, E.M., Brum, D., Gonzaga, L., Mauad, F. F., 2019. Evaluation of regression analysis and neural networks to predict total suspended solids in water bodies from unmanned aerial vehicle images. *Sustainability* 11, 2580. <https://doi.org/10.3390/su11092580>.
- Hafeez, S., Wong, M.S., Abbas, S., Jiang, G., 2021. Assessing the potential of geostationary Himawari-8 for mapping surface total suspended solids and its diurnal changes. *Remote Sens.* 13, 336. <https://doi.org/10.3390/rs13030336>.
- Harrington, Jr.J.A., Schiebe, F.R., Nix, J.F., 1992. Remote sensing of Lake Chicot, Arkansas: monitoring suspended sediments, turbidity, and Secchi depth with Landsat MSS data. *Remote Sens. Environ.* 39 (1), 15–27. [https://doi.org/10.1016/0034-4257\(92\)90137-9](https://doi.org/10.1016/0034-4257(92)90137-9).
- Hossain, A.K.M., Yafei, J., Xiaobo, C., 2010. Development of Remote Sensing Based Index for Estimating/Mapping Suspended Sediment Concentration in River and Lake Environments. In Proceedings of the 8th International Symposium on Ecohydraulics (ISE 2010) 0435, Zaragoza, Spain, 12–16 September 2010, pp. 578–585.
- Hossain, A., Mathias, C., Blanton, R., 2021. Remote sensing of turbidity in the Tennessee River using Landsat 8 satellite. *Remote Sens.* 13 (18), 3785. <https://doi.org/10.3390/rs13183785>.
- Hunter, P.D., Tyler, A.N., Carvalho, L., Codd, G.A., Maberly, S.C., 2010. Hyperspectral remote sensing of cyanobacterial pigments as indicators for cell populations and toxins in eutrophic lakes. *Remote Sens. Environ.* 114, 2705–2718. <https://doi.org/10.1016/j.rse.2010.06.006>.
- Ibrahim, H.D., Xue, P., Eltahir, E.A.B., 2020. Multiple salinity equilibria and resilience of Persian/Arabian Gulf Basin salinity to brine discharge. *Front. Mar. Sci.* 7, 573. <https://doi.org/10.3389/fmars.2020.00573>.
- Janadeleh, H., Jahangiri, S., Ali Kameli, M., 2018. Assessment of heavy metal pollution and ecological risk in marine sediments (a case study: Persian Gulf). *Hum. Ecol. Risk Assess.* 24 (8), 2265–2274. <https://doi.org/10.1080/10807039.2018.1443792>.
- Jensen, D., Simard, M., Cavanaugh, K., Sheng, Y., Fichot, C.G., Pavelsky, T., Twilley, R., 2019. Improving the transferability of suspended solid estimation in wetland and deltaic waters with an empirical hyperspectral approach. *Remote Sens.* 11, 1629. <https://doi.org/10.3390/rs11131629>.
- John, V.C., Coles, S.L., Abozed, A.I., 1990. Seasonal cycles of temperature, salinity and water masses of the western Arabian Gulf. *Oceanol. Acta* 13, 273–281. <https://archimer.ifremer.fr/doc/00131/24246/>.
- Kabir, S.M.I., Ahmari, H., 2020. Evaluating the effect of sediment color on water radiance and suspended sediment concentration using digital imagery. *J. Hydrol.* 589, 125189 <https://doi.org/10.1016/j.jhydrol.2020.125189>.
- Kampf, J., Sadrinasab, M., 2006. The circulation of the Persian Gulf: a numerical study. *Ocean Sci.* 2, 27–41. <https://doi.org/10.5194/os-2-27-2006>.
- Kavan, J., Wiczorek, I., Tallentire, G.D., Demidionov, M., Uher, J., Strzelecki, M.C., 2022. Estimating suspended sediment fluxes from the largest glacial Lake in Svalbard to Fjord System using Sentinel-2 data: Trebrevatnet case study. *Water* 14, 1840. <https://doi.org/10.3390/w14121840>.
- Kuhn, C., Valerio, A.M., Ward, N., Loken, L., Sawakuchi, H.O., Kampel, M., Richey, J., Stadler, P., Crawford, J., Striegl, R., Vermote, E., Pahlevan, N., Butman, D., 2019. Performance of Landsat-8 and Sentinel-2 surface reflectance products for river remote sensing retrievals of chlorophyll-a and turbidity. *Remote Sens. Environ.* 224, 104–118. <https://doi.org/10.1016/j.rse.2019.01.023>.
- Kutser, T., Paavel, B., Verpoorter, C., Ligi, M., Soomets, T., Toming, K., Casal, G., 2016. Remote sensing of black lakes and using 810 nm reflectance peak for retrieving water quality parameters of optically complex waters. *Remote Sens.* 8, 497. <https://doi.org/10.3390/rs8060497>.
- Lacaux, J., Tourre, Y., Vignolles, C., Ndione, J., Lafaye, M., 2007. Classification of ponds from high-spatial resolution remote sensing: application to Rift Valley Fever epidemics in Senegal. *Remote Sens. Environ.* 106, 66–74. <https://doi.org/10.1016/j.rse.2006.07.012>.
- Lardner, R., Lehr, W., Fraga, R., Sarhan, M., 1988. A model of residual currents and pollutant transport in the Arabian Gulf. *Appl. Math. Model.* 12, 379–390. [https://doi.org/10.1016/0307-904X\(88\)90067-4](https://doi.org/10.1016/0307-904X(88)90067-4).

- Lee, Z., Shang, S., Lin, G., Chen, J., Doxaran, D., 2016. On the modeling of hyperspectral remote-sensing reflectance of high-sediment-load waters in the visible to short wave infrared domain. *Appl. Opt.* 55, 1738–1750. <https://opg.optica.org/ao/abstract.cfm?URI=ao-55-7-1738>.
- Li, D., Anis, A., Senafi, F.A., 2020. Physical response of the northern Arabian Gulf to winter shamals. *J. Mar. Syst.* 203, 103280 <https://doi.org/10.1016/j.jmarsys.2019.103280>.
- Li, H.Y., Tan, Z., Ma, H., Zhu, Z., Abeshu, G.W., Zhu, S., Cohen, S., Zhou, T., Xu, D., Leung, L.R., 2022. A new large-scale suspended sediment model and its application over the United States. *Hydro. Earth Syst. Sci.* 26, 665–688. <https://doi.org/10.5194/hess-26-665-2022>.
- Liao, Y.P., Kaihatu, J.M., 2016a. Numerical investigation of wind waves in the Persian Gulf bathymetry effects. *J. Atmos. Ocean. Technol.* 33, 17–31. <https://doi.org/10.1175/JTECH-D-15-0066.1>.
- Liao, Y.P., Kaihatu, J.M., 2016b. The effect of wind variability and domain size in the Persian Gulf on predicting nearshore wave energy near Doha, Qatar. *Appl. Ocean Res.* 55, 18–36. <https://doi.org/10.1016/j.apor.2015.11.012>.
- Liu, H., Li, Q., Shi, T., Hu, S., Wu, G., Zhou, Q., 2017. Application of Sentinel 2 MSI images to retrieve suspended particulate matter concentrations in Poyang Lake. *Remote Sens.* 9, 761. <https://doi.org/10.3390/rs9070761>.
- Lodhi, M.A., Rundquist, D.C., Han, L., Kuzila, M.S., 1997. The potential for remote sensing of loess soils suspended in surface waters. *J. Am. Water Resour. Assoc.* 33 (1), 111–117. <https://doi.org/10.1111/j.1752-1688.1997.tb04087.x>.
- Lokier, S.W., Fiorini, F., 2016. Temporal evolution of a coastal system, Abu Dhabi, United Arab Emirates. *Mar. Geol.* 381, 102–113. <https://doi.org/10.1016/j.margeo.2016.09.001>.
- Long, C.M., Pavelsky, T.M., 2013. Remote sensing of suspended sediment concentration and hydrologic connectivity in a complex wetland environment. *Remote Sens. Environ.* 129, 197–209. <https://doi.org/10.1016/j.rse.2012.10.019>.
- Louis, J., Debaecker, V., Pflug, B., Main-Knorn, M., Bierniarz, J., Müller-Wilm, U., Cadau, E., Gascon, F., 2016. SENTINEL-2 SEN2COR: L2A processor for users. In: *Proc. 'Living Planet Symposium 2016', Prague, Czech Republic, 9–13 May 2016 (ESA SP-740, August 2016)*.
- Lymburner, L., Botha, E., Hestir, E., Anstee, J., Sagar, S., Dekker, A., Malthus, T., 2016. Landsat 8: providing continuity and increased precision for measuring multi-decadal time series of total suspended matter. *Remote Sens. Environ.* 185, 108–118. <https://doi.org/10.1016/j.rse.2016.04.011>.
- Lyons, M., Phinn, S., Roelfsema, C., 2011. Integrating Quickbird multi-spectral satellite and field data: mapping bathymetry, seagrass cover, seagrass species and change in Moreton Bay, Australia in 2004 and 2007. *Remote Sens.* 3, 42–64. <https://doi.org/10.3390/rs3010042>.
- McCullough, I.M., Loftin, C.S., Sader, S.A., 2012. High-frequency remote monitoring of large lakes with MODIS 500 m imagery. *Remote Sens. Environ.* 124, 234–241. <https://doi.org/10.1016/j.rse.2012.05.018>.
- McFeeters, S.K., 1996. The use of normalized difference water index (NDWI) in the delineation of open water features. *Int. J. Remote Sens.* 17, 1425–1432. <https://doi.org/10.1080/01431169608948714>.
- Mohsen, A., Kovács, F., Kiss, T., 2022. Remote sensing of sediment discharge in rivers using Sentinel-2 images and machine-learning algorithms. *Hydrology* 9, 88 (doi: 10.3390/h9).
- Montalvo, L.G., 2010. Spectral analysis of suspended material in coastal waters: A comparison between band math equations. Available online: <https://docplayer.net/39330139-Spectral-analysis-of-suspended-material-in-coastal-waters-a-comparison-between-band-math-equations.html> (accessed on 13 January 2021).
- Moore, S.A., Le Coz, J., Hurther, D., Paquier, A., 2012. On the application of horizontal ADCPs to suspended sediment transport surveys in rivers. *Cont. Shelf Res.* 46, 50–63. <https://doi.org/10.1016/j.csr.2011.10.013>.
- Mora, S., Fowler, S.W., Wyse, E., Azemard, S., 2004. Distribution of heavy metals in marine bivalves, fish and coastal sediments in the Gulf and Gulf of Oman. *Mar. Pollut. Bull.* 49 (5–6), 410–424. <https://doi.org/10.1016/j.marpolbul.2004.02.029>.
- Moses, W.J., Gitelson, A.A., Berdnikov, S., Povazhnyy, V., 2009. Satellite estimation of chlorophyll-a concentration using the red and NIR bands of MERIS-the Azov Sea case study. *IEEE Geosci. Remote Sens. Lett.* 6, 845–849. <https://doi.org/10.1109/lgrs.2009.2026657>.
- Nechad, B., Ruddick, K., Park, Y., 2010. Calibration and validation of a generic multi-sensor algorithm for mapping of total suspended matter in turbid waters. *Remote Sens. Environ.* 114, 854–866. <https://doi.org/10.1016/j.rse.2009.11.022>.
- Pahlevan, N., Chittimalli, S.K., Balasubramanian, S.V., Vellucci, V., 2019. Sentinel-2/Landsat-8 product consistency and implications for monitoring aquatic systems. *Remote Sens. Environ.* 220, 19–29. <https://doi.org/10.1016/j.rse.2018.10.027>.
- Pahlevan, N., Smith, S., Alikas, K., Anstee, J., Barbosa, C., Binding, C., Bresciani, M., Cremella, B., Giardino, C., Gurlin, D., Fernandez, V., Jamet, C., Kangro, K., Lehmann, M.K., Loisel, H., Matsushita, B., Hä, N., Olmanson, L., Potvin, G., Simis, S. G.H., VanderWoude, A., Vantrepotte, V., Ruiz-Verdúr, A., 2022. Simultaneous retrieval of selected optical water quality indicators from Landsat-8, Sentinel-2, and Sentinel-3. *Remote Sens. Environ.* 270, 112860 <https://doi.org/10.1016/j.rse.2021.112860>.
- Park, E., Latrubesse, E.M., 2014. Modeling suspended sediment distribution patterns of the Amazon River using MODIS data. *Remote Sens. Environ.* 147, 232–242. <https://doi.org/10.1016/j.rse.2014.03.013>.
- Park, H.B., Lee, G.H., 2016. Evaluation of ADCP backscatter inversion to suspended sediment concentration in estuarine environments. *Ocean Sci. J.* 51, 109–125. <https://doi.org/10.1007/s12601-016-0010-3>.
- Peterson, K.T., Sagan, V., Sidike, P., Cox, A.L., Martinez, M., 2018. Suspended sediment concentration estimation from Landsat imagery along the lower Missouri and middle Mississippi Rivers using an extreme learning machine. *Remote Sens.* 10, 1503. <https://doi.org/10.3390/rs10101503>.
- Pous, S., Carton, X.J., Lazure, P., 2013. A process study of the wind-induced circulation in the Persian Gulf. *Open J. Mar. Sci.* 3, 1–11. <https://doi.org/10.4236/ojms.2012.24016>.
- Pous, S., Lazoure, P., Carton, X., 2015. A model of the general circulation in the Persian Gulf and in the Strait of Hormuz: intraseasonal to interannual variability. *Cont. Shelf Res.* 94, 55–70. <https://doi.org/10.1016/j.csr.2014.12.008>.
- Purkis, S.J., Riegl, B.M., 2012. Geomorphology and reef building in the SE gulf. In: Riegl, B., Purkis, S. (Eds.), *Coral Reefs of the Gulf. Coral Reefs of the World*, vol. 3. Springer, Dordrecht. [https://doi.org/10.1007/978-94-007-3008-3\\_3](https://doi.org/10.1007/978-94-007-3008-3_3).
- Purkis, S., Rivers, J., Strohmenger, C.J., Warren, C., Yousif, R., Ramirez, L., Riegl, B., 2017. Complex interplay between depositional and tectrophysical environments in Holocene tidal carbonates (Al Ruwais, Qatar). *Sedimentology* 64 (6), 1646–1675. <https://doi.org/10.1111/sed.12368>.
- Rai, A.K., Kumar, A., 2015. Continuous measurement of suspended sediment concentration: technological advancement and future outlook. *Measurement* 76, 209–227. <https://doi.org/10.1016/j.measurement.2015.08.013>.
- Rajendran, S., Al Kuwari, H.A., Sadooni, F.N., Nasir, S., Govil, H., 2021a. Remote sensing of inland Sabkha and study of salinity and temporal stability for sustainable development: A case study from the West coast of Qatar. *Sci. Total Environ.* 782, 146932 <https://doi.org/10.1016/j.scitotenv.2021.146932>.
- Rajendran, S., Al-Khayat, J.A., Veerasingam, S., Nasir, S., Vethamony, P., Sadooni, F.N., Al Kuwari, H.A., 2021b. WorldView-3 mapping of Tarmat deposits of the Ras Rakan Island, Northern Coast of Qatar: environmental perspective. *Mar. Pollut. Bull.* 163, 111988 <https://doi.org/10.1016/j.marpolbul.2021.111988>.
- Rajendran, S., Al-Naimi, N., Al Khayat, J.A., Sorino, C.F., Sadooni, F.N., Al Kuwari, H.A., 2022. Chlorophyll-a concentrations in the Arabian Gulf waters of arid region: a case study from the northern coast of Qatar. *Reg. Stud. Mar. Sci.* <https://doi.org/10.1016/j.rjsma.2022.102680>.
- Randazzo, G., Barreca, G., Cascio, M., Crupi, A., Fontana, M., Gregorio, F., Lanza, S., Muziarfuti, A., 2020. Analysis of very high spatial resolution images for automatic shoreline extraction and satellite-derived bathymetry mapping. *Geosciences* 10, 172. <https://doi.org/10.3390/geosciences10050172>.
- Riegl, B.M., Purkis, S.J., 2012. Coral reefs of the gulf: adaptation to climatic extremes in the world's hottest sea. In: Riegl, B., Purkis, S. (Eds.), *Coral Reefs of the Gulf*. In: *Coral Reefs of the World*, vol. 3. Springer, Dordrecht. [https://doi.org/10.1007/978-94-007-3008-3\\_1](https://doi.org/10.1007/978-94-007-3008-3_1).
- Rivers, J.M., Skeat, S.L., Yousif, R., Liu, Stanmore, E., Tai, P., Al-Marri, S.M., 2019. The depositional history of near-surface Qatar aquifer rocks and its impact on matrix flow and storage properties. *Arab. J. Geosci.* 12, 380. <https://doi.org/10.1007/s12517-019-4498-6>.
- Rivers, J.M., Dalrymple, R.W., Yousif, R., Al-Shaikh, I., Butler, J.D., Warren, C., Skeat, S. L., Abdel Bari, E.M.M., 2020. Mixed siliciclastic-carbonate-evaporite sedimentation in an arid eolian landscape: the Khor Al Adaid tide-dominated coastal embayment, Qatar. *Sediment. Geol.* 408, 105730 <https://doi.org/10.1016/j.sedgeo.2020.105730>.
- Rumora, L., Miler, M., Medak, D., 2020. Impact of various atmospheric corrections on Sentinel-2 land cover classification accuracy using machine learning classifiers. *ISPRS. Int. J. Geo-Inf.* 9, 277. <https://doi.org/10.3390/ijgi9040277>.
- Saberion, M., Brom, J., Nedbal, V., Souček, P., Císař, P., 2020. Chlorophyll-a and total suspended solids retrieval and mapping using Sentinel-2A and machine learning for inland waters. *Ecol. Indic.* 113, 106236 <https://doi.org/10.1016/j.ecolind.2020.106236>.
- Schmugge, T.J., Kustas, W.P., Ritchie, J.C., Jackson, T.J., Rango, A., 2002. Remote sensing in hydrology. *Adv. Water Resour.* 25 (8–12), 1367–1385. [https://doi.org/10.1016/S0309-1708\(02\)00065-9](https://doi.org/10.1016/S0309-1708(02)00065-9).
- Shahzad, M.I., Meraj, M., Nazeer, M., Zia, I., Inam, A., Mehmood, K., Zafar, H., 2018. Empirical estimation of suspended solids concentration in the Indus Delta Region using Landsat-7 ETM+ imagery. *J. Environ. Manag.* 209, 254–261. <https://doi.org/10.1016/j.jenvman.2017.12.070>.
- Sharples, J., Middelburg, J.J., Fennel, K., Jickells, T.D., 2017. What proportion of riverine nutrients reaches the open ocean? *Glob. Biogeochem. Cycles* 31, 39–58. <https://doi.org/10.1002/2016GB005483>.
- Sillanpää, M., Ncibi, M.C., Matilainen, A., Vepsäläinen, M., 2018. Removal of natural organic matter in drinking water treatment by coagulation: A comprehensive review. *Chemosphere* 190, 54–71. <https://doi.org/10.1016/j.chemosphere.2017.09.113>.
- Silveira Kuppsinskü, L., Thomassim Guimarães, T., Menezes de Souza, E., Zanotta, D., C., Roberto Veronez, M., Gonzaga Jr., L., Mauad, F.F., 2020. A method for chlorophyll-a and suspended solids prediction through remote sensing and machine learning. *Sensors* 20, 2125. <https://doi.org/10.3390/s20072125>.
- Smith, B., Pahlevan, N., Schalles, J., Ruberg, S., Errera, R., Ma, R., Giardino, C., Bresciani, M., Barbosa, C., Moore, T., Fernandez, V., Alikas, K., Kangro, K., 2021. A chlorophyll-a algorithm for Landsat-8 based on mixture density networks. *Front. Remote Sens.* 1, 623678 <https://doi.org/10.3389/frsen.2020.623678>.
- Steinmetz, F., Deschamps, P.-Y., Ramon, D., 2011. Atmospheric correction in presence of sun glint: application to MERIS. *Opt. Express* 19, 9783–9800. <https://doi.org/10.1364/OE.19.009783>.
- Tessier, C., Le Hir, P., Lurton, X., Castaing, P., 2008. Estimation of suspended sediment concentration from backscatter intensity of Acoustic Doppler Current Profiler. *Compt. Rendus Geosci.* 340 (1), 57–67. <https://doi.org/10.1016/j.crte.2007.10.009>.
- Thoppil, P.G., Hogan, P.J., 2010. Persian gulf response to a wintertime Shamal wind event. *Deep-Sea Res.* 57, 946–955. <https://doi.org/10.1016/j.dsr.2010.03.002>.
- Toming, K., Kutser, T., Laas, A., Sepp, M., Paavel, B., Nges, T., 2016. First experiences in mapping lake water quality parameters with Sentinel-2 MSI imagery. *Remote Sens.* 8, 640. <https://doi.org/10.3390/rs8080640>.

- Torres-Vera, M.A., 2023. Mapping of total suspended solids using Landsat imagery and machine learning. *Int. J. Environ. Sci. Technol.* <https://doi.org/10.1007/s13762-023-04787-y>.
- Townshend, J.R., Justice, C.O., 1986. Analysis of dynamics of African vegetation using the normalised difference vegetation index. *Int. J. Remote Sens.* 7, 1435–1445. <https://doi.org/10.1080/01431168608948946>.
- Tucker, C.J., Sellers, P.J., 1986. Satellite remote sensing of primary productivity. *Int. J. Remote Sens.* 7, 1395–1416. <https://doi.org/10.1080/01431168608948944>.
- Tuuli, S., Kristi, U., Dainis, J., Agris, B., Matiss, Z., Tiit, K., 2020. Validation and comparison of water quality products in Baltic Lakes using sentinel-2 MSI and sentinel-3 OLCI data. *Sensors* 20 (3), 742. <https://doi.org/10.3390/s20030742>.
- Vanacker, V., 2011. Suspended sediment concentration. In: Singh, V.P., Singh, P., Haritashya, U.K. (Eds.), *Encyclopedia of Snow, Ice and Glaciers*. Encyclopedia of Earth Sciences Series. Springer, Dordrecht. [https://doi.org/10.1007/978-90-481-2642-2\\_560](https://doi.org/10.1007/978-90-481-2642-2_560).
- Vaughan, G.O., Burt, J.A., 2016. The changing dynamics of coral reef science in Arabia. *Mar. Pollut. Bull.* 105, 441–458. <https://doi.org/10.1016/j.marpolbul.2015.10.052>.
- Virtanen, O., Constantinidou, E., Tyystjarvi, E., 2020. Chlorophyll does not reflect green light – how to correct a misconception. *J. Biol. Educ.* 56, 552–559. <https://doi.org/10.1080/00219266.2020.1858930>.
- Wang, J.J., Lu, X.X., 2010. Estimation of suspended sediment concentrations using Terra MODIS: an example from the lower Yangtze River, China. *Sci. Total Environ.* 408, 1131–1138. <https://doi.org/10.1016/j.scitotenv.2009.11.057>.
- Wilson, K.L., Wong, M.C., Devred, E., 2022. Comparing Sentinel-2 and WorldView-3 imagery for coastal bottom habitat mapping in Atlantic Canada. *Remote Sens.* 14, 1254. <https://doi.org/10.3390/rs14051254>.
- Xu, H., 2006. Modification of normalized difference water index (NDWI) to enhance open water features in remotely sensed imagery. *Int. J. Remote Sens.* 27, 3025–3033. <https://doi.org/10.1080/01431160600589179>.
- Xu, M., Liu, H., Beck, R., Lekki, J., Yang, B., Shu, S., Kang, E.L., Anderson, R., Johansen, R., Emery, E., Reif, M., Benko, T., 2019. A spectral space partition guided ensemble method for retrieving chlorophyll-a concentration in inland waters from Sentinel-2A satellite imagery. *J. Gt. Lakes Res.* 45 (3), 454–465. <https://doi.org/10.1016/j.jglr.2018.09.002>.
- Youssef, M., El-Sorogy, A., Al Kahtany, K., Al Otiaby, N., 2015. Environmental assessment of coastal surface sediments at Tarut Island, Arabian Gulf (Saudi Arabia). *Mar. Pollut. Bull.* 96 (1–2), 424–433. <https://doi.org/10.1016/j.marpolbul.2015.05.010>.
- Yu, Y., Notaro, M., Kalashnikova, O.V., Garay, M.J., 2016. Climatology of summer Shamal wind in the Middle East. *J. Geophys. Res. Atmos.* 121, 289–305. <https://doi.org/10.1002/2015JD024063>.
- Yunus, A.P., Masago, Y., Hijioaka, Y., 2021. Analysis of long-term (2002–2020) trends and peak events in total suspended solids concentrations in the Chesapeake Bay using MODIS imagery. *J. Environ. Manag.* 299, 113550. <https://doi.org/10.1016/J.JENVMAN.2021.113550>.
- Yunus, A.P., Masago, Y., Boulange, J., Hijioaka, Y., 2022. Natural and anthropogenic forces on suspended sediment dynamics in Asian estuaries. *Sci. Total Environ.* 836, 155569. <https://doi.org/10.1016/j.scitotenv.2022.155569>.
- Zhang, C., Liu, Y., Chen, X., Gao, Y., 2022. Estimation of suspended sediment concentration in the Yangtze Main stream based on Sentinel-2 MSI data. *Remote Sens.* 14, 4446. <https://doi.org/10.3390/rs14184446>.